RÔMULO DIAS NOVAES

EFEITOS DA INFECÇÃO EXPERIMENTAL COM *Trypanosoma cruzi* SOBRE A MORFOLOGIA E FUNÇÃO CARDÍACA E PANCREÁTICA DE RATOS WISTAR

Tese apresentada à Universidade Federal de Viçosa, como parte das exigências do Programa de Pós-Graduação em Biologia Celular e Estrutural, para obtenção do título de *Doctor Scientiae*.

VIÇOSA

MINAS GERAIS – BRASIL

2012

Ficha catalográfica preparada pela Seção de Catalogação e Classificação da Biblioteca Central da UFV

T

N935e
2012

Novaes, Rômulo Dias, 1983-
Efeitos da infecção experimental com *Trypanosoma cruzi* sobre a morfologia e função cardíaca e pancreática de ratos Wistar / Rômulo Dias Novaes. – Viçosa, MG, 2012.
viii, 66f. : il. (algumas col.) ; 29cm.

Orientador: Izabel Regina dos Santos Costa Maldonado
Tese (doutorado) - Universidade Federal de Viçosa.
Inclui bibliografia.

1. Chagas, Doença de. 2. Coração - histopatologia. 3. Coração. 4. Morfologia. 5. Miocárdio - Doenças - Tratamento. 6. Exercícios físicos - Aspectos fisiológicos. 7. Rato como animal de laboratório. 8. Pâncreas. 9. Pâncreas - Doenças. I. Universidade Federal de Viçosa. II. Título.

CDD 22. ed. 616.9363

RÔMULO DIAS NOVAES

EFEITOS DA INFECÇÃO EXPERIMENTAL COM *Trypanosoma cruzi* SOBRE A MORFOLOGIA E FUNÇÃO CARDÍACA E PANCREÁTICA DE RATOS WISTAR

Tese apresentada à Universidade Federal de Viçosa, como parte das exigências do Programa de Pós-Graduação em Biologia Celular e Estrutural, para obtenção do título de *Doctor Scientiae*.

APROVADA: 17 de setembro de 2012.

_____ _____

Ana Cristina Rodrigues Lacerda Cristiane Alves Silva Menezes

_____ _____

Leandro Licursi de Oliveira Márcia de Carvalho Vilela

_____

Izabel Regina dos Santos Costa Maldonado
(Orientadora)

A minha amada mãe Cláudia pela luta incessante, amor incondicional e pela representação de um modelo de inspiração.

AGRADECIMENTOS

À Universidade Federal de Viçosa e ao Programa de Pós-Graduação em Biologia Celular e Estrutural, pelo apoio em minha formação pessoal e profissional.

À CAPES, pelo apoio financeiro.

À minha orientadora Profª. Izabel Regina dos Santos Costa Maldonado, pelo acolhimento de um recém-chegado à UFV, pelos ensinamentos, confiança, paciência e apoio em questões pessoais e profissionais.

Aos meus Coorientadores Prof. Clóvis Andrade Neves e Prof. Antônio José Natali, pelos ensinamentos, paciência e disposição em ajudar.

Ao Prof. André Talvani Pedrosa, pelo apóio na inoculação dos animais, disposição em ajudar e incentivo para continuar a caminhada.

À Profª. Ana Cristina Rodrigues Lacerda, pela disposição em participar da banca examinadora e por representar um modelo de busca pela integração entre a pesquisa e a prática docente.

À Profª. Cristiane Alves Silva Menezes, pela disposição em participar da banca examinadora.

Ao Prof. Leandro Licursi de Oliveira, pela disposição em participar da banca examinadora, pelos conselhos em pesquisa, e pela solicitude em ajudar e abrir as portas do seu laboratório para a realização de experimentos.

À Profª. Maria do Carmo Gouveia Peluzio por seus conselhos, ótima convivência e pelo apoio nas análises de estresse oxidativo.

Ao Prof. Sérgio Luis Pinto da Matta pela ótima parceria nos trabalhos de pesquisa, sua alegria contagiante, e ensinamentos que levarei por toda a vida pessoal e profissional.

Ao Prof. Clóvis Andrade Neves pelos conselhos pessoais e profissionais, pela confiança no nosso trabalho de equipe e solicitude em ajudar.

Ao Prof. José Eduardo Serrão pelos estímulos constantes para a busca de qualidade de pesquisa, pelo apoio de infraestrutura e financeiro para a utilização dos laboratórios da UFV e realização das análises de microscopia eletrônica.

À Profª. Sílvia Pompolo, por gentilmente permitir a utilização de seu laboratório para aquisição das imagens utilizadas.

A todos os professores do Programa de Pós-Graduação em Biologia Celular e Estrutural, por todos os ensinamentos e incentivo.

A todos os funcionários do Programa de Pós-Graduação em Biologia Celular e Estrutural, em especial Beth e Diana, pela ótima convivência, paciência e auxílio em todos os momentos necessários.

Aos amigos do laboratório de Biologia Estrutural: Kener, Marlí, Wagner, Márcia, Edson, Daniel, Maria do Carmo, Marcília, Marcelo, Suzana, Andréa, Rafael, Daiane e Lílian, pela disposição em ajudar, pelas conversas e momentos de descontração, pela companhia na luta do dia-a-dia e pelo incentivo constante.

Aos amigos Carla Veloso Gonçalves Ribeiro e Gilmar Edilberto Valente pelo apoio profissional, disponibilidade em ajudar, confiança no trabalho que realizamos e oportunidade de dividir alguns bons momentos juntos.

Ao companheiro de trabalho e amigo Alex Bhering por iluminar nossos caminhos em meio aos procedimentos e técnicas em histologia, pela paciência, pela companhia e pelos momentos de descontração.

Á amiga de Viçosa Marisa, pelo acolhimento e apoio nas horas de necessidade.
As amigas Arlete e Reggiani pela parceria, momentos de descontração e apoio pessoal e profissional.

Aos amigos do coração que fazem o dia-a-dia mais feliz mesmo que a distância nos separe de alguns: Aline, Ana Izaura, Arlete, Eliziária, Kener e Reggiani.

À minha mãe e meu pai por tudo que fizeram por mim e que me permitiu chegar até aqui.

À Deus, pela minha vida e pela força para superar as dificuldades e continuar a caminhada.

ÍNDICE

RESUMO

NOVAES, Rômulo Dias, D.Sc., Universidade Federal de Viçosa, setembro de 2012. **Efeitos da infecção experimental com *Trypanosoma cruzi* sobre a morfologia e função cardíaca e pancreática de ratos Wistar**. Orientadora: Izabel Regina dos Santos Costa Maldonado. Coorientadores: Antônio José Natali e Clóvis Andrade Neves.

O *Trypanosoma cruzi,* um protozoário parasita intracelular, é o agente causador da doença de Chagas, que acomete vários órgãos, principalmente o coração. Nessa doença, modificações na biomecânica de cardiomiócitos e no metabolismo glicêmico de repouso e durante o exercício físico têm sido raramente relatadas. Assim, o presente estudo investigou os efeitos da infecção experimental com *T. cruzi* sobre a morfofisiologia cardíaca e pancreática em ratos Wistar. A relação entre função pancreática e a tolerância ao exercício nesses animais foi adicionalmente analisada. Vinte e oito ratos Wistar machos foram divididos em um grupo não infectado (n=14) e um grupo infectado (n=14). Após nove semanas da inoculação com formas tripomastigotas de *T. cruzi*, os animais foram submetidos a um protocolo incremental de corrida para avaliação do desempenho físico. Em seguida, os corações e pâncreas foram removidos para a análise histopatológica, estereológica e bioquímica. Cardiomiócitos foram isolados por dispersão enzimática para análise das propriedades biomecânicas. Os resultados demonstraram que a infecção com *T. cruzi* induziu alterações morfológicas no coração e pâncreas, manifestando-se como focos inflamatórios difusos, atrofia e morte celular, necrose e fibrose tecidual. Os animais infectados apresentaram aumento da oxidação de lipídeos e proteínas no coração e pâncreas, respectivamente. Esses animais demonstraram alteração na cinética de glicose em repouso e durante o exercício, redução da tolerância ao exercício e disfunção biomecânica em ambos os componentes de contração e relaxamento dos cardiomiócitos. Não houve alteração do número de células β nas ilhotas pancreáticas ou modificação na proporção de minerais no tecido cardíaco dos animais infectados. Assim, os resultados indicaram que a infecção com *T. cruzi* é capaz de induzir modificações patológicas na estrutura e função cardíaca e pancreática conduzindo a disfunções na biomecânica de cardiomiócitos e no metabolismo glicêmico, eventos potencialmente relacionados à reduzida tolerância ao exercício físico em ratos.

ABSTRACT

NOVAES, Rômulo Dias, D.Sc., Universidade Federal de Viçosa, September, 2012. **Effects of experimental *Trypanosoma cruzi* infection on the cardiac and pancreatic morphology and function in Wistar rats.** Adviser: Izabel Regina dos Santos Costa Maldonado. Co-advisers: Antônio José Natali and Clóvis Andrade Neves.

Trypanosoma cruzi, an intracellular protozoan parasite, is the causative agent of Chagas' disease, which impair several organs, mainly the heart. In this disease, changes in cardiomyocytes biomechanics and glucose metabolism at rest and during exercise have been rarely reported. Thus, the present study investigated the effects of experimental *T. cruzi* infection on the cardiac and pancreatic morphophysiology in rats Wistar. The relationship between pancreatic function and exercise tolerance in these animals it was additionally analyzed. Twenty-eight male Wistar rats were divided into an uninfected (n=14) and an infected group (n=14). After nine weeks of inoculation with trypomastigote forms of *T. cruzi*, animals were subjected to an incremental running protocol to evaluate the physical performance. Then, hearts and pancreases were removed for histopathological, stereological and biochemical analysis. Cardiomyocytes were isolated by enzymatic dispersion for analysis of biomechanical properties. The results showed that *T. cruzi* infection induced morphological changes in the heart and pancreas, which were evidenced by diffuse inflammatory foci, atrophy and cell death, necrosis and tissue fibrosis. Infected animals presented increased oxidation of lipids and proteins in the heart and pancreas, respectively. These animals showed changes in glucose kinetics at rest and during exercise, reduced exercise tolerance and biomechanical dysfunction in both components of contraction and relaxation of cardiomyocytes. There was no change in the number of β cells in the pancreatic islets or modification in the proportion of minerals in the cardiac tissue from infected animals. Thus, the results indicated that *T. cruzi* infection is able to induce pathological changes in the cardiac and pancreatic structure and function, conducing to dysfunctions in cardiomyocytes biomechanics and glucose metabolism, events potentially related to the reduced exercise tolerance in rats.

Artigo 1

Use of fluorescence in a modified *disector* method to estimate the myocytes number in cardiac tissue

Rômulo Dias Novaes,[1] Arlete Rita Penitente,[1] André Talvani,[2] Antônio José Natali,[1] Clóvis Andrade Neves,[1] Izabel R.S.C. Maldonado,[1]

[1]Federal University of Viçosa, MG, Brazil;
[2]Federal University of Ouro Preto, MG, Brazil;

Running title: Fluorescence to estimate cardiomyocytes number

Key-words: cardiomyocytes, fluorescence microscopy, morphology.

***Address for correspondence:** Izabel Regina dos Santos Costa Maldonado, Universidade Federal de Viçosa, Departamento de Biologia Geral. Edifício Chotaro Shimoya, Avenida PH Rolfs, s/nº, CEP: 35.570-000 Viçosa, Minas Gerais, MG, Brasil. Tel: +55 (031) 3899-3365. **Email**: irscosta@ufv.br

Abstract

Study basis: Currently, conventional *disector* methods require a considerable financial, technical and operational cost to estimate the cells quantity, including cardyomyocytes, in a 3D area.

Objective: to use fluorescence microscopy in a modified *disector* method to determine myocytes number in cardiac tissue in normal and pathological conditions.

Methods: Were used four-month-old male Wistar rats with weight of 366.25 ± 88.21g randomized in control (CG, n=8) and infected (IG, n=8) groups. IG animals were inoculated with *T. cruzi* Y strain (300,000 trypomastigotes/50g wt). After eight weeks, the animals were weighted and euthanized. The left ventricles (LV) were removed for stereological analysis of numerical density of cardiomyocytes (Nv[c]) and total number of these cells in the LV (N[c]). These parameters were estimated using a fluorescent *disector* (FD) and compared with the conventional optical (OD) and physical (PD) *disector* methods.

Results: In both *disector* methods, IG animals presented significant decrease of Nv[c] and N[c] compared to CG animals ($P < 0.05$). There was no significant difference in these variables despite the *disector* method applied in CG and IG animals ($P > 0.05$). A strong correlation, equal or above 96%, was obtained between FD, OD and PD.

Conclusion: The FD method seems to be equally reliable to determine Nv[c] and N[c] in normal and pathological conditions and present some advantages compared to conventional *disector* methods: reduction of histological slices and images in the stereological analysis, reduction of time to analyze the images, construction of FD in simple microscopes using the epifluorescence mode, distinction of *disector* planes in lower magnifications.

Introduction

Over the past years a great effort was made to develop a reliable and reproducible method to estimate the number of particles in organs and tissues, but, until 1984 all these methods had intrinsic bias[1-3]. In 1984, Sterio described several modifications in the approaches used to estimate the objects quantity in three-dimensional space and introduced the *disector* method[4]. Currently, most authors consider the *disector* method unbiased and the well-established theoretical background makes the method largely acceptable[5-7].

The *disector* may be obtained through two different methods that are based in the same theoretical principles and basic requirements to estimate the particles quantities. These methods are the optical and physical disector[4,8-10]. Although both the methods have reduced the bias of particle quantity estimation, they still required the acquisition of a large number of histological images and a great deal of time to perform the counts. Particularly, the optical *disector* also require a light microscope of high cost adapted with axis-Z mobile stage[11]. Moreover, the physical *disector* are extremely laborious because require serial histological sections and images with a perfect alignment in the different parallel sections[3,10].

Considering that the aim of the sampling design for stereology is to obtain the maximal amount of quantitative structural information at a given total cost, time or effort, the purpose of this study was to use fluorescence microscopy in a modified *disector* method to determine myocytes number in cardiac tissue on normal and pathological conditions. Thus, a murine model of *T. cruzi* infection that recognizably conduces to disruption of cardiac myocytes and modifies the number of these cells in the myocardium was used[12]. We hypothesized that the proposed method may reduce the operational cost observed in the conventional methods as well as maintain the accuracy of the cell quantity measurements.

Materials and methods

Animals and experimental groups

Four-month-old male Wistar rats with initial weight of 366.25 ± 88.21 g were provided with rodent chow and water *ad libitum* and maintained in animal facilities with a controlled environment (temperature at 22 ± 3 ºC, humidity at 60 - 70 % and 12 hour light/dark inverted cycles). The samples size were determined considering the probability P=1/2 to

occur increase or decrease of the variables of interest. Thus, considering the significance level α=0.05, the minimal significant number of animals used in statistical analysis was: P=(1/2)events; so, if n=5, P=(1/2)5 or P=0.03; thus, P<0.05[10]. Due to the intrinsic variability of the parasitism in target organs and the mortality associated with *T. cruzi* infection a correction factor of 50% was incorporated to the initial calculation, determining samples of 8 animals, randomly allocated into control (CG, n= 8) and infected (IG, n= 8) groups.

Infection

Animals from IG were inoculated intraperitoneally with *T. cruzi* Y strain (300,000 trypomastigotes/50g body weight in 1 mL of infected mice blood[13]. Infection was confirmed four days post-inoculation by the presence of trypomastigotes in peripheral blood collected from the rat's tail as described by Brener[14]. All experimental procedure were conducted in accordance with the Brazilian College of Animal Experimentation and approved by the Animal Research Ethics Commission of the Veterinary Department at the Federal University of Viçosa, Brazil (protocol number 30/2009).

Biometrical analysis

Eight weeks after inoculation the animals were euthanized under anesthesia and the hearts were removed. The left ventricles (LV) were dissected and weighed separately. The LV volume was obtained by the submersion method, where the liquid displacement from the organ volume is weighed. Due to the specific gravity (σ) of isotonic saline is 1.0048, the volume is obtained by: volume= weight/σ, or simply volume (10^3 mm^3) $\approx$ weight (g)[15]. The LV weight and volume was determined including the interventricular septum.

Tissue processing and determination of histological areas

The atria and ventricles were put into histological fixative for 48 hours (freshly prepared 10% w/v formaldehyde in 0.1 M phosphate buffer pH 7.2)[16,17]. The fragments of LV were obtained through the *orientator* method to define isotropic and uniform random sections (IUR) required in the stereological study[3]. These fragments were dehydrated in ethanol,

cleared in xylol and embedded in paraffin. Blocks were cut into 3 μm sections and stained by hematoxylin-eosin (H&E) or 4',6-diamidino-2-phenylindole at 0.2% (DAPI)[18].

The representative number of *disectors* used in stereological analysis for each animal was determined considering the stabilization of the coefficient of variation (CV) of myocytes nuclei number in crescents random samples of *disectors* (5, 10, 15, 20 and 25). Thus, was calculated the arithmetical mean and the respective CV for each sample size. When the increase of *disector* numbers resulting in no significant difference of CV between 3 consecutive samples, the smallest sample size was considered as the minimal representative19. Using this method, the variation of myocytes nuclei number was stabilized from the sample of 10 *disectors*.

Optical and physical *disector* methods

Sections stained with H&E were mounted on histology slides using Entelan® mounting medium (Merk, Darmstadt, Germany) and the images were captured using a light microscope (Olympus BX-60®, Tóquio, Japan) connected to a digital camera (Olympus QColor-3®, Tokyo, Japan). Observation was made with a ×100 planachromatic immersion oil objective (NA= 1.25) to clearly identified cardiomyocyte (*cmy*) nuclei boundaries[16,17].

The number of cardiomyocyte nuclei (*cmyn*) in a 3-dimensional probe was estimated using the optical (OD) and physical (PD) *disector* methods3. The *disector* consists of 2 parallel planes aimed at sampling ‘‘top points’’ of particles in between. Sampling volume was created with 2 parallel sections separated by 3 μm (*h*) and 2 reference planes both containing a test frame (AT). In both *disector* methods, a pair of photomicrographs separated by *h* distance is used to form the two reference planes. In the OD, the parallel photomicrographs are obtained in the same histological area adjusting the focal plane (*h*= 3 μm) using the micrometrical screw. In the PD, two serial sections are obtained in the microtome (*h*= 3 μm) and the same histological area is photographed in both sections, supplying two photomicrographs physically separated.

Fluorescent *disector* method

In the fluorescent *disector* method (FD), sections stained with DAPI were mounted on histology slides using 50% sucrose solution in distillated water (w/v). Images were captured in an epifluorescence mode of the same microscope using a HBO 100 mercury

lamp and a filter for dye excitation at 365 nm and a light emission at 460 nm. Observation was made with the same 100× planachromatic lens previously described. In this method, using the 3 μm (*h*) sections, the two reference planes required to delimitate the *disector* are obtained in a unique image and pars of photomicrographs are not required as in the conventional methods. Furthermore, the *cmyn* presents in all thickness of the section may be observed inside or outside of the focal plane. To avoid repeat cells count, sections were obtained in semi-series, using 1 in every 20 sections. The FD was additionally obtained with a ×40 objective lens only to demonstrate the possibility of applying the method using smaller magnifications.

Estimation of numerical density and total number of cardiomyocytes

The numerical density of *cmyn* (Nv[c], *cmyn* per mm3) was determined from 10 random *disector* pairs for each animal, being defined as Nv[*c*]= *Q*-[*cmyn*] / *h*×AT ; where *Q*- represents the number of profiles of *cmyn* counted in the test area on the *disector* reference section (‘‘look up’’ plane)3,17. In the FD, the *Q*- value in the Nv[*c*] formula was multiplied by a correction factor of 0.5 to avoid overestimation of the measures. The total number of *cmyn* in the LV (N[c]) was estimated as the product of Nv[c] / LV volume. The counts were performed in an AT= 2670 μm2. All stereological analysis was performed using the software Image Pro-Plus 4.5® (Media Cybernetics, Silver Spring, USA).

Statistical analysis

All analyses were performed using the statistical platform GraphPad Prism (version 5.01, GraphPad Software, San Diego, CA). Data are expressed as mean and standard deviation (mean ± S.D.)[16,17]. The normality of the data distribution was verified using the Kolmogorov-Smirnov test. Based in this test, data of weight and volume were compared using the t-test. The Mann-Whitney U test was used to compare the stereological data between the groups. The disector methods were compared using the Kruskal-Wallis test and correlating using the *Spearman's* method. Statistical significance was established at α= 0.05.

Results

There was no statistical difference in body mass (CG, 502.17 ± 57.76 g vs. IG, 494.69 ± 87.90 g; P> 0.05) and left ventricle volume (CG, 456.47 ± 26.18 mm3 vs. IG, 487.69 ± 34.89 mm3; P> 0.05) between the groups.

Histopathological analysis of the LV showed a marked diffuse inflammatory infiltrate in IG. Moreover, was observed in this group a disorganization of histological structure with an increased interstitial area and a larger distance between the ventricular myocytes. These cells also showed an increased cross-sectional area and some these presented a narrowing of cytoplasm region induced by a large amount of *T. cruzi* amastigote forms (Fig. 1).

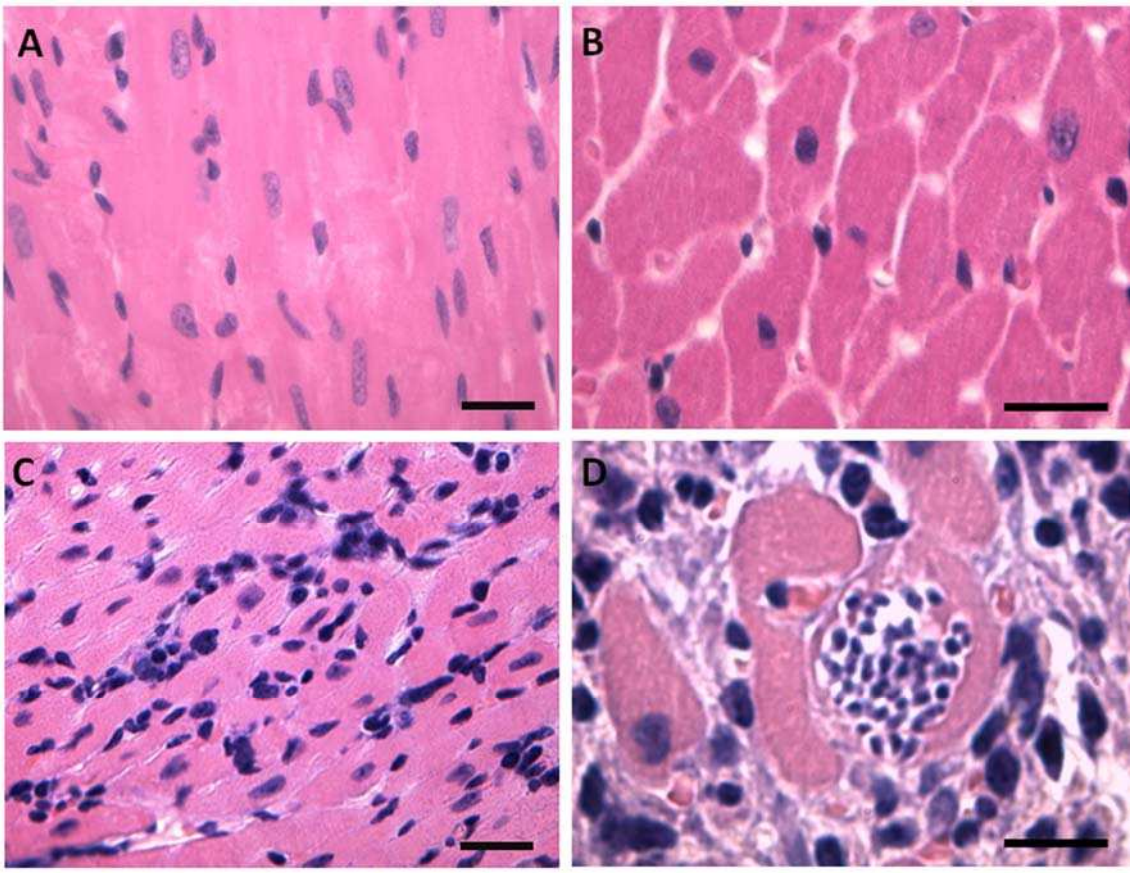

Fig. 1. Representative photomicrographs of the left ventricle from control (A and B) and infected (C and D) groups. The infected animals were inoculated intraperitoneally with *T. cruzi* Y strain (300,000 trypomastigotes/50 g body weight). (A) Myocardial longitudinal section showing a well-organized structure (magnification ×400, bar = 15µm, H&E stain). In B is observed a myocardial cross-section showing reduced interstitial space and a close relation between the myocytes (magnification ×1000, bar = 15µm, H&E stain). (C) Longitudinal section showing a diffuse inflammatory infiltrate and a disorganization of

myocardium structure (magnification ×400, bar = 15µm, H&E stain). In D panel are observed diffuse inflammatory infiltrate with evident increase of the interstitial space and the myocyte diameter. In this panel is observed a large number of amastigote forms of *T. cruzi* in the myocyte cytoplasm (magnification ×1000, bar = 15µm, H&E stain).

The conventional OD is represented in the fig. 2. In this method, the disector was obtained in the same microscopic image adjusting the Z axis of microscope to create an optical separation of 3 µm between the images. In the physical method (image not show) the *disector* was obtained using the microscopic images of two different serial histological sections physically separated at the same distance as in the OD (3 µm).

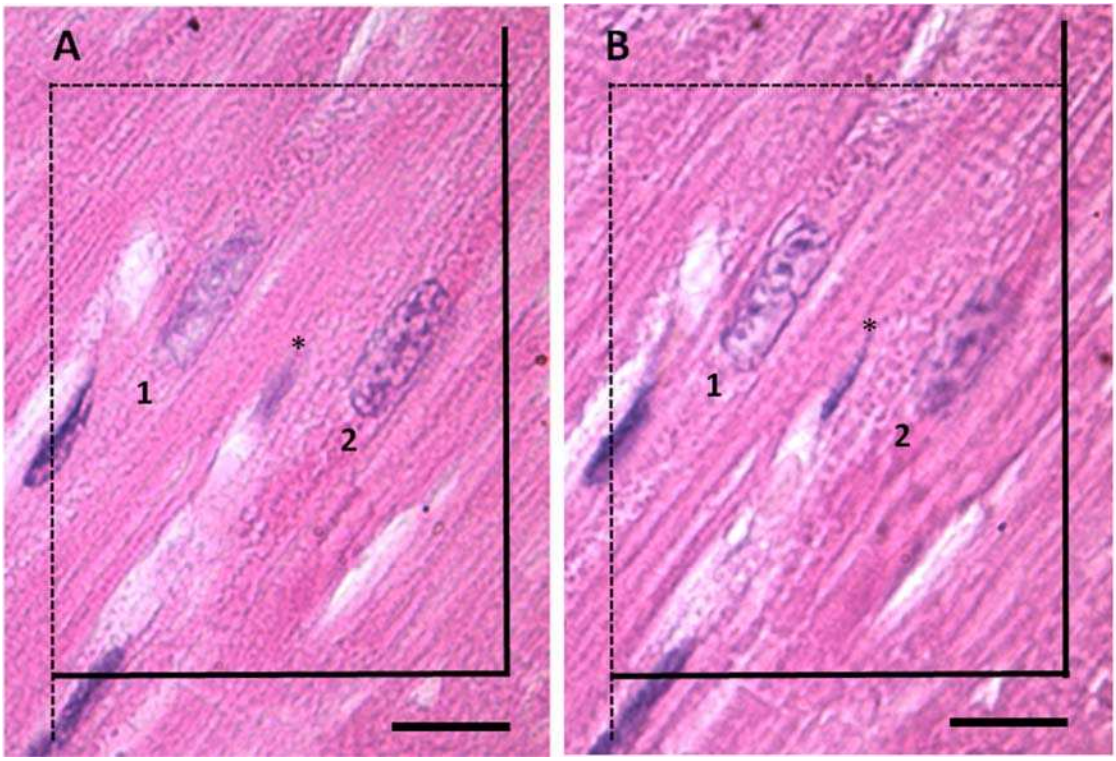

Fig. 2. Representative photomicrographs of the two *disector* focal planes separated by 3 µm of distance (*h*). *Disector* is the union of a reference plane with an unbiased counting frame of area (AT) and a look-up plane at distance *h* apart. Cardiomyocyte nuclei (*cmyn*) are counted or sampled because 1) they are hit by reference plane, 2) their transects are captured by the counting frame in there, and 3) they are not hit by ‘‘look-down’’ plane and in the forbidden edge of AT (thick edge). (A) There are two *cmyn* into the frame of the ‘‘look-up’’ plane (numbered) and only the *cmyn* 2 should be counted. In this plane, we also observe the shadow of the other *cmyn* (1) and a fusiform fibroblast nuclei (*) that are not

counted because they violate at least 1 of the 3 preceding requirements. (B) The *cmyn* 1, is in the focus of the ‘‘look-down’’ plane and the *cmyn* 2 is a shadow outside the focus. If *h* and AT is known the *disector* volume is determined. Dividing the number of counted nuclei by this volume, a direct estimate of Nv[c] is obtained (magnification ×1000, bar= 15µm, H&E stain).

The proposed *disector* method, named fluorescent *disector* (FD), is represented in the fig. 3. In this method, the *disector* was obtained in the same microscopic image thought the differential fluorescence emission by the *cmyn*. While in the OD and PD a total of 160 photomicrographs (80 *disector* pairs) were required in the stereological analysis, in FD a half of microscopic images (80 individual *disectors*) were used.

In the FD was incorporated a correction factor of 50% in the formula used to determine Nv[c] in OD and PD. Thus, the formula used to estimate Nv[c] in the FD was Nv[*c*]= *Q*-[*cmyn*] × 0.5 / *h*×AT; where the constant 0.5 was established to avoid overestimation of *cmyn* count in FD.

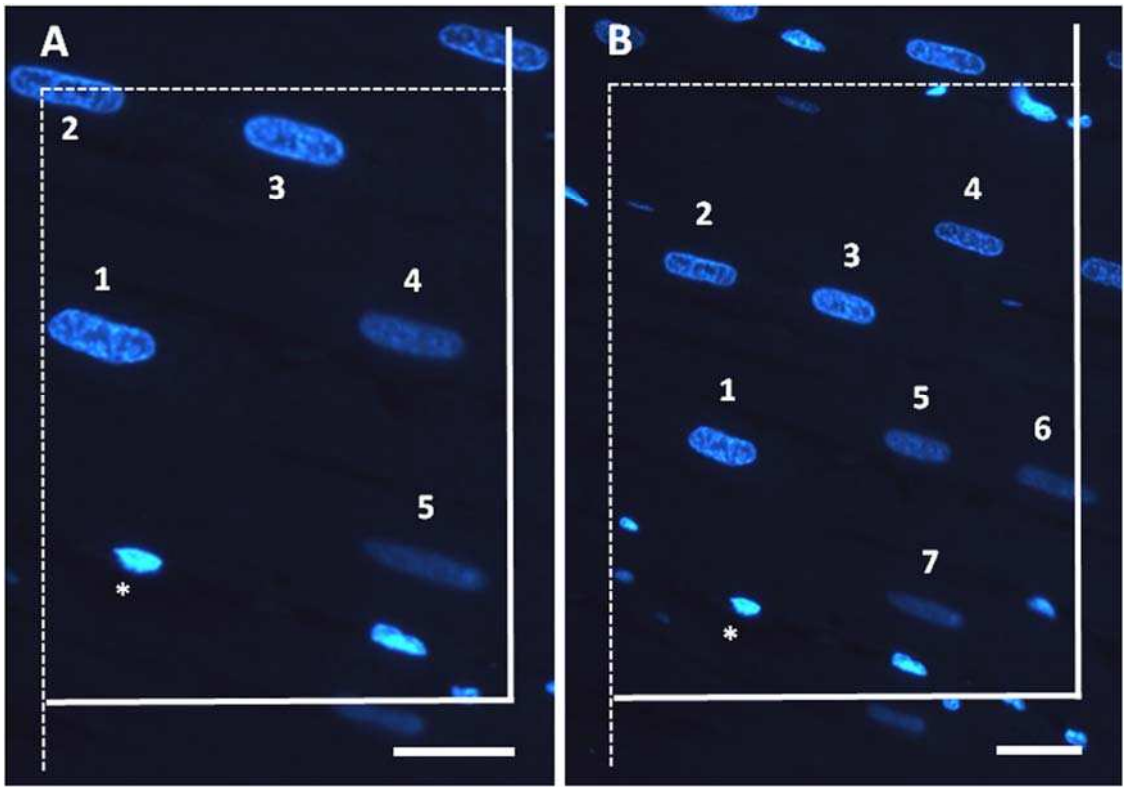

Fig. 3. Representative photomicrograph of the fluorescent *disector* method obtained using ×100 (A) and ×40 (B) objective lens. In this method, two different focal planes are formed in the same microscopic image thought the differential fluorescence emission by the

cardiomyocyte nuclei (*cmyn*). Superficial *cmyn* (look up plane) appears in the focal plane with more brightness, and *cmyn* in deep planes (look down plane) is observed outside the focal plane with low bright. The unions of these reference planes at distance *h* apart with an unbiased counting frame of area (AT) constitute a Fluorescent *disector* (FD). (A) The *cmyn* 1, 2 and 3 in the ‘‘look-up’’ plane may be counted and the nuclei 4 and 5 are in look down plane and not may be counted. Fibroblast nuclei are indicated by asterisk (magnification ×1000, bar= 15µm, 6-diamidino-2-phenylindole stain). (B) There are four *cmyn* into the frame in the ‘‘look-up’’ plane (1, 2, 3 and 4) that may be counted. The *cmyn* 5, 6 are observed in look down plane and the nucleus 7 hit on forbidden edge of AT. Thus these not may be counted because violate the requirements to count (magnification ×400, bar= 15µm, 6-diamidino-2-phenylindole stain). The same principles to *cmyn* count described to the conventional *disector* are used in this method.

The results of Nv[c] and N[c] obtained using the different *disector* methods are showed in the table 1. In both *disector* methods, the infected animals presented significant decrease of both variables compared to control animals. There was no significant difference in these variables values despite the *disector* methods used.

Table 1. Numerical density and absolute number of cardiomyocytes in the left ventricular myocardium from control and infected rats.

	OD	**PD**	**FD**
Nv[c] / mm3			
Control	175424.64 ± 6135.36	183977.32 ± 9162.78	172429.44 ± 8123.37
Infected	90771.41 ± 3314.30*	95352.20 ± 3144.13*	91141.127 ± 3741.09*
N[c] x 104			
Control	7948.51 ± 471.45	8302.75 ± 519.98	8017.90 ± 474.789
Infected	4665.58 ± 318.99*	5042.18 ± 371.44*	4969.99 ± 354.77*

Data are expressed as mean ± S.D. OD, Optical *disector*; PD, Physical *disector*; FD, Fluorescent *disector*; Nv[c], numerical density of cardiomyocytes; N[c], absolute number of cardiomyocytes. All values were obtained using a ×100 objective lens (magnification

×1000). *, denotes statistical difference from CG (P< 0.01), Mann-Whitney U test. There are no statistical differences between the *disector* methods, Kruskal-Wallis test.

The result of correlation analysis of the Nv[c] and N[c] obtained using the different *disector* methods is presented in the table 2. A strong, direct and significant correlation was obtained in all correlations between both the methods.

Table 2. Correlations between the results of numerical density and absolute number of left ventricular myocytes obtained using different *disector* methods in control and infected rats.

	Nv[c] / mm3		**N[c]**	
	Correlation (r)	P value	Correlation (r)	P value
Control				
OD x PD	0.98	<0.0001	0.98	<0.0001
OD x FD	0.96	<0.0001	0.97	<0.0001
PD x FD	0.96	<0.0001	0.96	<0.0001
Infected				
OD x PD	0.99	<0.0001	0.99	<0.0001
OD x FD	0.97	<0.0001	0.98	<0.0001
PD x FD	0.97	<0.0001	0.97	<0.0001

OD, Optical *disector*; PD, Physical *disector*; FD, Fluorescent *disector*; Nv[c], numerical density of cardiomyocytes; N[c], absolute number of cardiomyocytes. The results are relative to the data obtained using a ×100 objective lens (magnification ×1000). Correlations were tested using the *Spearman's* method.

Discussion

For many years, the morphological studies of biological tissues were based in ambiguous histopathological descriptions. Initially, the use symbols representation to indicate the increase or decrease of a variable is the best way to express the data in a semi-

quantitative context[20]. With the refinement these morphological approaches, was incorporated in the histological and pathological analysis the use of a two-dimension (2D) quantitative system to describe the morphometrical characteristics of organs and tissues[1,21,22]. These refinements introduced significant advances in histo-quantitative studies. However, the estimation of microscopic parameters in a three-dimension (3D) space remained as an issue still not well resolved, and the conventional morphometric methods present intrinsic bias that reduced the reliability of the morphological measurements[2,3,23].

Considering the intrinsic bias of several morphometrical measurements, calculations of probability statistics and geometry applied in geology and other soil sciences were adapted to the study of biological materials[1,24], forming the basis of actual stereology3. The development of stereology constitutes an important evolution in the histo-quantitative methods, allowing the development of more accurate and reliable morphological data[9,10,25,26].

The objects quantity estimation in biological tissue has been a crucial issue in morphological studies and diagnostic pathology, constituting the more refined measures in stereology[3,7]. The development of *disector* methods by Sterio in 1984 led to a creative and relatively simple way to estimate the particle number in an organ or tissue4. However, the *disector* methods still require a series of technical requirements that increase the time and cost of data acquisition[5,8,10]. The need to obtain and analyze a large number of microscopic images is a common limitation of both OD and PD methods, especially when several groups and tissue samples are studied at once. Moreover, the costs to acquisition or adaptation of a microscope with controlled Z axis contribute to limit the application of OD11. On other hand, obtain a PD is extremely laborious because involve the quality of the microtomy, appropriated processing of serial sections and technical ability to determine a perfect alignment of these sections4. Furthermore, minimal alignment error can lead to a bias in the cell count characterized by an overestimation or underestimation of stereological outcomes. Thus, these conventional *disector* methods still require a considerable financial, technical and operational cost to estimate the particle quantity in a 3D area[11].

The present study proposes an alternative method to estimate myocytes quantity in the cardiac tissue using fluorescence microscopy in a modified *disector* method. The construction of a FD was based in the similar requirements to particle counts described in the conventional disector methods. However, an adaptation of the formula to determine

N[c] was required in FD. The introduction of a correction factor was necessary to reduce the overestimation of the measurements. In the conventional methods, the particle count results exclude those which hit the forbidden plane (generally look down plane), contributing to reduce the measurement bias[27,28]. As in the FD the presence or absence of the same particle cannot be observed in both *disector* planes, as occurs in OD and PD, the calculation of probability determine a 0.5 correction factor to the N[c] formula, considering 50% of chance of a particle is observed or not in both planes.

The application of the FD using the proposed method provided similar results of Nv[c] and N[c] in relation the other *disector* methods, without significant difference between the methods. Both methods presented sufficient sensibility to determine the reduction of left ventricle myocyte number in the murine model of cardiac infection *T. cruzi*-induced. This model was selected to the present study because of the well-established tropism to cardiac tissue presented by this parasite and its ability to reduce the number of myocytes due to parasite replication, differentiation and cell evasion, which propagates in an ongoing destructive process[12,13]. In addition, the correlations between the FD with the conventional methods were strong, indicating that the FD method may be equally reliable to estimate the myocytes number in cardiac tissue. The reliability of the measures seems to be maintained in both health and pathological conditions.

Although the FD also constitute an optical method, the present study demonstrated that the FD also may be obtained using objective lens with lower magnifications (×40) compared with the conventional lens (×100) required in OD. In OD, lower magnifications are not often used because determine a large depth-of-field, fact that difficult the acquisition of different *disector* focal planes (look up and look down) because it maintains all section structures inside the focus, despite of the Z axis adjust3.

Conclusion

The FD described in the present study offered an alternative method to estimate myocytes quantity in cardiac tissue. This method seems to be equally reliable in normal and pathological conditions to determine the same parameters of Nv[c] and N[c] obtained using the conventional *disector* methods. Although the results has been similar between the three methods, the FD showed some advantages compared to OD and PD such as: 1) reduction (by half) of the number of histological slices and images required in the stereological analysis, 2) reduction of time to analyze the required images, 3) construction

of FD in simple microscopes using the epifluorescence mode, 4) distinction of the *disector* look up and look down planes using lower magnifications, 5) reliability of stereological results demanding reduced technical and operational cost in relation to the OD and PD methods.

Conflict of interest

There is no conflict of interest.

References

1. Weibel ER, Kistler GS, Scherle WF. Practical stereological methods for morphometric cytology. J Cell Biol. 1966; 30(1):23-38.
2. Aherne WA. Methods of counting discrete tissue components in microscopical sections. J R Micr Soc. 1967; 87(3):493-501.
3. Mandarim-de-Lacerda CA. Stereological tools in biomedical research. An Acad Bras Cienc 2003; 75(4):469-86.
4. Sterio DC. The unbiased estimation of number and sizes of arbitrary particles using the disector. J Microsc. 1984;134(Pt2):127-136.
5. Dorph-Petersen KA, Nyengaard JR, Gundersen HJ. Tissue shrinkage and unbiased stereological estimation of particle number and size. J Microsc. 2001; 204(Pt3):232-246.
6. Charleston LB, Thyer AC, Klein NA, Soules MR, Charleston JS. An improved method for the production of slides from oversized samples of glycol methacrylate-embedded tissues: Application for optical disector based stereology. J Histotechnol 2003; 26(1): 49-52.
7. Eisele JC, Schaefer I-M, Nyengaard JR, Post H, Liebetanz D, Brüel A, et al. Effect of voluntary exercise on number and volume of cardiomyocytes and their mitochondria in the mouse left ventricle. Basic Res Cardiol. 2008; 103(1):12-21.

8. Gundersen HJ, Bagger P, Bendtsen TF, Evans SM, Korbo L, Marcussen N, et al. The new stereological tools: disector, fractionator, nucleator and point sampled intercepts and their use in pathological research and diagnosis. APMIS. 1988; 96(10):857-881.

9. Weibel ER. Measuring through the microscope: development and evolution of stereological methods. J Microsc. 1989; 155(Pt3):393-403.

10. Cruz-Orive LM, Weibel ER. Recent stereological methods for cell biology: a brief survey. Am J Physiol. 1990; 258(4 Pt1):148-156.

11. Xavier-Vidal R. Disector Z-axis mechanical method for stereology. An Acad Bras Cienc. 2010; 82:539-544.

12. Marin-Neto JA, Cunha-Neto E, Maciel BC, Simões MV. Pathogenesis of chronic Chagas' heart disease. Circulation 2007; 115(9):1109-1123.

13. Martinelli PM, Camargos ERS, Azevedo AA, Chiari E, Morel G, Machado CRS. Cardiac NGF and GDNF expression during Trypanosoma cruzi infection in rats. Auton Neurosci. 2006; 130(1-2):32-40.

14. Brener Z. Therapeutic activity and criterion of cure on mice experimentally infected with *Trypanosoma cruzi*. Rev Inst Med Trop São Paulo. 1962; 4:389-396.

15. Scherle W. A simple method for volumetry of organs in quantitative stereology. Mikroskopie. 1970; 26(1):57-63.

16. Xavier-Vidal R, Neves MC, Villar VC, Viana WN, Mandarim-de-Lacerda CA. Estereologia do miocárdio em fetos humanos. Estudo quantitativo das modificações estruturais nos dois últimos trimestres de gestação. Arq Bras Cardiol. 1993; 60(4):221-224.

17. Xavier-Vidal R, Madi K. Comparação entre os miocárdios ventriculares direito e esquerdo durante período fetal humano. Uma avaliação estereológica. Arq Bras Cardiol. 1999; 72(5):581-586.

18. Masotti L, Cavatorta P, Avitabile M, Barcellona ML, von Berger J, Ragusa N. Characterization of 4'-6 diamidino-2 phenylindole (DAPI) as a fluorescent probe of DNA structure. It J Biochem. 1982; 31(2):90-99.

19. Moro L, Vasconcelos AC, Santos FGA, Alves CM, Nunes JES, Sampaio IBM. Determination of the minimal representative number of microscopical fields to quantify apoptosis in canine lymph nodes. Arq Bras Med Vet Zootec. 2004; 56(3):408-410.

20. Bucher O. Contribution on the method of morphometry. Anat Anz. 1967; 120(1), 39-40.

21. Rohr H. Principles, possibilities of use and limits of morphometry. Acta Histochem. 1976; 16:83-89.

22. Rohr H, Oberholzer M, Barstsch G, Keller M. Morphometry in experimental pathology: methods, baseline data and applications. Int Rev Exp Pathol. 1976; 15:233-325

23. Elias H, Hyde DM. A guide to practical stereology. 1st ed. NewYork: Karger, 1983.

24. Chalkley HW. Methods for quantitative morphological analysis of tissue. J Natl Cancer Inst. 1943; 4:47-53.

25. Collan Y. Stereology in diagnostic pathology. Pathologica 1997; 89:462-466.

26. Von Bartheld C. Counting particles in tissue sections: choices of methods and importance of calibrationto minimize biases. Histol Histopathol. 2002; 17(2):639-648.

27. Weibel ER. Stereological Methods: practical methods for biological morphometry. 1st ed. London: Academic Press, 1979.

28. Mouton PR. Principles and practices of unbiased stereology. An introduction for bioscientist. 1st ed. Baltimore: John Hopkins University Press, 2002.

Artigo 2

Trypanosoma cruzi infection alters glucose metabolism at rest and during exercise without modifying the morphology of pancreatic islets in rats

Rômulo D. Novaes[a], Reggiani V. Gonçalves[b], Arlete R. Penitente[a], André Talvani[c], Maria C.G. Peluzio[d], Clóvis A. Neves[a], Antônio J. Natalie, and Izabel R.S.C. Maldonado[a]

[a]Department of General Biology, Federal University of Viçosa, Viçosa, MG, Brazil

[b]Department of Morphology, Federal University of Pelotas, Pelotas, RS, Brazil

[c]Department of Biological Sciences and NUPEB, Federal University of Ouro Preto, Ouro Preto, MG, Brazil

[d]Department of Nutrition and Health, Federal University of Viçosa, MG, Brazil

[e]Department of Physical Education, Federal University of Viçosa, Viçosa, MG, Brazil

Correspondence: Izabel R.S.C Maldonado, Federal University of Viçosa, Department of Physical Education. Av. Peter Henry Rolfs, s/nº, Zip code: 35.570-000. Viçosa-MG, Brasil. Phone: +55 31 3899-4390. Fax: +55 31 3899-2249. E-mail: irscosta@ufv.br

Abstract

This study investigated the effects of *Trypanosoma cruzi* infection on pancreatic morphology and glucose metabolism at rest and during exercise. Wistar rats were randomized into control (CG=10) and infected (IG=10) groups. The IG animals were inoculated with *Trypanosoma cruzi* Y strain (300,000 trypomastigotes/50 g). After 9 weeks the animals were subjected to glucose (OGTT) and insulin (ITT) tolerance tests and a treadmill running protocol. Blood glucose, lactate and time to fatigue were determined. After euthanasia, the pancreases were removed for morphological and biochemical analyses. The IG presented abnormal glucose kinetics in OGTT and a similar glucose curve in ITT compared to the CG. During the exercise test the IG showed anticipation of time to fatigue. At the point of fatigue no difference was found in blood glucose and lactate between the groups. There was significant correlation between lactate levels and the time to fatigue. The IG presented marked pancreatic inflammation, fibrosis and protein oxidation. The number of β cells in the IG animals was not reduced. *Trypanosoma cruzi* infection impaired pancreas morphology and glucose metabolism at rest and during exercise in rats, which could constitute an additional mechanism in the induction of exercise intolerance in Chagas' disease.

Key-words: Chagas' disease, glucose metabolism, pancreas, pathology, exercise.

Introduction

Chagas' disease (ChD) is a neglected illness caused by the intracellular protozoan parasite *Trypanosoma cruzi* (*T. cruzi*), which remains as an important health problem in 18 developing countries in South and Central America [4,28]. Its main clinical manifestations are cardiac and/or digestive disturbances, with a prevalence of about 12-14 million cases worldwide [28].

Although there is sufficient evidence showing that *T. cruzi* is able to spread and infect several organs such as the gonads, kidney, liver and pancreas in humans [30,32] and animals [7,33,34], these infection sites have not been researched to the same extent as cardiac and intestinal manifestations, and thus remain neglected. Some studies addressed the involvement of the pancreas in ChD [7,30,32-34]. Traditionally, this observation has been based on evidence of altered glucose and insulin responses after oral glucose tolerance tests in chronic chagasic patients and *post-mortem* histopathological analyses of the pancreas [18,35,37]. Although the direct pathological and functional repercussions of *T. cruzi* on the heart and gut are the primary focus of investigations and interventions in ChD [4,28], it is evident that pancreatic infections also present an important clinical significance in this disease [26,35]. This importance is clear according to the concept of the enteroinsular axis, considering the interrelationships of pancreatic secretions and the intestinal tube in several peptidergic routes that participate in the metabolism of energy substrates [8]. In fact, it has been shown that patients with the digestive form of chronic Chagas' disease frequently present variable degrees of pancreatic morphological changes and glucose metabolism dysfunctions [18,26]. In addition, previous studies suggested that chagasic individuals present permanently elevated blood glucose levels and a high predisposition toward the development of type 2 diabetes mellitus (DM2) compared to healthy subjects [18,26,35].

Glucose is an important compound related to exercise performance under healthy and diseased conditions [37]. Clinical investigations have shown that chagasic subjects present a reduced functional capacity and exercise tolerance [10,16,17,20]. However, few studies have evaluated the factors that affect the capacity to perform physical exercise in patients with ChD, and exercise intolerance has primarily been associated with changes in the mechanical and electrical activities of cardiac and skeletal muscle tissues [10,16,17,20,23]. Currently, several aspects of the pathogenesis of exercise intolerance in ChD still need to be clarified. To the best of our knowledge up to the present date no studies on humans or

animal models have been carried out to investigate blood glucose levels during exercise in *T. cruzi* infection. Thus, the present study was designed to investigate the effects of *T. cruzi* infection on pancreatic morphology and glucose metabolism at rest and during exercise and the relationship between these variables and exercise tolerance. We hypothesized that the dysfunction in glucose metabolism might be an additional component involved in reduced exercise tolerance in rats.

Materials and Methods

Animals and infection

Twenty 4-month-old male Wistar rats (*Rattus norvegicus*) with an initial weight of 366.25 ± 31.17 g were used in the experiments and were provided with a rodent diet (AIN-93M) [29] and water *ad libitum*. The animals were divided into an uninfected control group (CG, n=10) and an infected group (IG, n=10) and maintained under a controlled environment with a temperature of 22 ± 2 ºC and 12-h light/dark cycles. The rats of the IG were inoculated intraperitoneally with 1 mL of infected mice blood containing the *T. cruzi* Y strain (300,000 trypomastigotes/50 g body weight), according to the method of Martinelli et al. [22]. Infection was confirmed by the presence of trypomastigotes in peripheral blood aliquots collected 4 days after inoculation [3]. All animals were euthanized 9 weeks after inoculation by cervical dislocation while under anesthesia. The experimental protocols were conducted in accordance with the Brazilian College for Animal Experimentation and were approved by the Animal Research Ethics Committee from the Federal University of Viçosa, Brazil (protocol 30/2009).

Body mass and underweight

Before being euthanized, the height and weight of the animals were measured to determine the body mass and calculate the Lee index. The Lee index is an indicator of underweight, estimated by the formula $\sqrt[3]{\text{body mass (g)}}$ / snout-anus length (cm) [1].

Pancreatic function and insulin tolerance

The oral glucose tolerance test (OGTT) was used to investigate pancreatic function through the insulin response induced by a glycemic load. Prior to the OGTT all rats were fasted for 16 h, although water was not restricted. Then, anhydrous glucose was orally administered to the animals (3 g/kg of body weight) diluted in 3 mL distilled water (w/v) with a feeding syringe. Blood samples were collected by tail vein puncture at 0 (fasting glucose), 30, 60, 90 and 120 min after the glucose load to determine blood glucose via the glucose oxidase method (OneTouch Ultra®, Jonson & Jonson, CA, USA). The area under the blood glucose response curve (AUC) was calculated for each animal using the trapezoidal method [27].

Forty-eight hours after OGTT, the insulin tolerance test (ITT) was performed to investigate the peripheral tolerance to insulin. Before the ITT the animals were fasted for 2 h to eliminate any differences in stomach contents or plasma insulin between the rats. The rats were injected subcutaneously at the back of the neck with 0.5 units/kg insulin (Biochemica, Florida, USA) and the blood glucose was measured at the same times described for the OGTT (0, 30, 60, 90 and 120 min) using the same glucose oxidase method. The ratio of the glucose decay constant (KITT) was calculated using the formula 0.693/(T1/2), where the T1/2 of plasma glucose was determined from the glucose curve during its phase of linear decay (0-30 min) [9].

Exercise test protocol and metabolic parameters

Each rat was subjected to an aerobic running test until fatigue 48 h after the ITT, according to the incremental running protocol described by Koch and Britton [14]. Prior to the exercise test the rats were familiarized with the motor-driven treadmill (Insight Instruments®, Ribeirão Preto, SP, Brazil) by running at a speed of 10 m/min-1 at a 5% inclination for 5 min per day for 7 consecutive days. This amount of exposure to treadmill running is slightly below that required to produce metabolic adaptations [14]. The test was performed at a constant slope of 5% with a starting speed of 10 m/min-1. The treadmill velocity was increased by 1 m/min^{-1} every 2 min and each rat was run until fatigued. Fatigue was defined as the point at which the animals were no longer able to keep pace with the treadmill [15]. Immediately before and after the test, the blood levels of lactate and glucose were measured using reflectance photometry (Accutrend Lactate®, Roche,

Basel, Switzerland) and glucose oxidase (OneTouch Ultra®, Jonson & Jonson, CA, USA), respectively. The distance traveled (m) and time to fatigue (min) were also recorded.

Protein oxidation, fibrosis

The protein carbonyl content was measured using the 2,4-dinitrophenylhydrazine (DNPH) procedure [38]. Total protein levels in the lung tissue were measured using the Bradford method [2].

For each group, 20 sections of 8-μm thickness stained with Sirius red and Fast green were used to quantify the amount of collagen and total protein in pancreatic tissue using a previously described spectrophotometric method [19]. In this method, the maximal absorbance of Sirius red (540 nm) and Fast green (605 nm) dyes corresponds to the amount of collagen and non-collagen proteins, respectively.

Histological processing, histochemistry and immunohistochemistry

After the animals were euthanized each pancreas and liver were removed *in totum* and placed in histological fixative for 48 h (freshly prepared 10% w/v formaldehyde in 0.1 M phosphate buffer, pH 7.2). Pancreas and liver fragments were dehydrated in ethanol, cleared in xylol and embedded in paraffin. Blocks were cut into 4 and 8-μm sections and mounted on histological slides. The pancreas sections were stained by hematoxylin-eosin (H&E), Fast green and Sirius red for histopathological analysis and aldehyde-fuchsin [11] and indirect immunoperoxidase to localize the insulin-producing β cells that were evaluated in the stereological and kariometric analysis. According direct peroxidase technique [39], the sections were subjected to immunohistochemistry using anti-insulin monoclonal antibodies (lot number A90-117p-4, Bethyl Laboratory, Montgomery, TX, USA). The optimum dilution of the primary antibody was 1:500 and for the secondary antibody conjugated with peroxidase it was 1:200. The liver sections were stained with the best carmine method for glycogen [25]. Digital images were captured using a light microscope (Olympus BX-60®, Tóquio, Japan) connected to a digital camera (Olympus QColor-3®, Tokyo, Japan).

Histopathology, stereology and karyometry

The inflammatory process was evaluated by determining the relationship between the total number of polymorphonuclear (PMN) and mononuclear (MN) cells observed in the pancreas of control and infected animals [5]. These cells were evaluated in a test area of 3.4×103 μm^2 at a magnification of ×1000 across five random, non-coincident microscopic fields for each animal and a total of 170×10^3 μm^2 of pancreas tissue for each group [12]. All morphological analyses were performed using the image analysis software Image Pro-Plus 4.5® (Media Cybernetcs, Silver Spring, MD, USA).

The stereological parameters analyzed were: (A) the volume density (Vv) of the islets in pancreatic tissue (Vvi) and β cells per islet (Vvc); (B) the number of β cells per islet area (NAC) and islet volume (NVC); and (C) the islet volume (Vi). The point-counting method was used to estimate the parameters of item A using the formula Vv [structure] = *PP* [structure] / *PT*; where *PP* is the number of points that hit the structure and *PT* is the total number of test points [21]. For this analysis, Vvi was estimated using a test system of 200 points in a standard test area of 73×10^3 μm^2 across five random, non-coincident microscopic fields for each animal and a total of 3.6×106 μm^2 of pancreas tissue for each group. The relationship between the number of points of the test system that hit the islet profile and those that specifically hit β cells was used to calculated Vvc. A total of 100 islet profiles of the pancreas were examined in order to estimate items B and C. The Vvi was investigated under a magnification of ×40 and the other parameters were determined under a magnification of ×400.

The density of β cells per islet profile (NAC, β cells/μm2) was calculated by dividing the number of nuclei per islet profile by the mean islet area. The nuclear profiles were counted using the direct counting method under a magnification of ×200. The islet area (Ai) was measured directly using the image contour function of the Image Pro-Plus 4.5® software (Media Cybernetcs, Silver Spring, MD, USA). The numerical density of β cells per unit volume of islet cells (NVC, β cells/μm^3) was determined using a physical dissector (*d*) method. In this method the distance between look-up and look-down sections (t) was 3μm for each pair *d*. Thus, β cells seen in lookup in anterior sections but not the look-down sections were counted (Qn), and the numerical density of islets (NVC) was estimated as: NVC = Qn / Ai × t; where Ai is the islet area observed in sections of thickness t (3μm). The absolute number of β cells per islet (N, β cell/islet) was determined by multiplying

NVC by the islet volume. The islet volume (Vi) was calculated using Cavalieri's principle: $Vi = \Sigma t \times \Sigma Ai$ [21].

Sections stained with aldehyde-fuchsin were used for the karyometric study of β-cell nuclei. In the karyometric analysis 50 β cell nuclei for each animal were analyzed under a magnification of ×400. Using a calibrated linear scale the longest axis (D) and shortest axis (d) of the β cells were measured. The geometric axis of the nucleus (Dn) was calculated using the equation $Dn = (D \times d)^{1/2}$. This parameter was used to calculate the nuclear volume from the formula $V = \pi/6 \times Dn$ [31].

In liver sections stained with the carmine method, the volume density of glycogen cytoplasmic inclusions in the histological area (Vv[*glyc*], %) was estimated according a stereological protocol previously described [25].

Statistical analysis

The data are presented as the mean ± standard deviation (mean ± SD). Normal distribution of the data was verified using the Kolmogorov-Smirnov test. The blood glucose, lactate, protein carbonyl levels and index of inflammatory processes were compared using the Student's t-test. Stereological and karyometric data were compared using the Mann-Whitney U test. The relationship between blood glucose, lactate and total time to fatigue was assessed by linear regression. A probability of $p<0.05$ was considered statistically significant.

Results

Body mass, underweight and liver glycogen

No statistical difference was found between the groups for body mass (CG, 502.17 ± 20.41 g *vs.* IG, 494.69 ± 31.06 g), Lee index (CG, 311.89 ± 17.93 *vs.* IG, 300.04 ± 13.21), or the volume density of glycogen inclusions in the liver tissue (CG, 16.38 ± 4.03% *vs.* IG, 17.10 ± 5.57%) (Fig. 1).

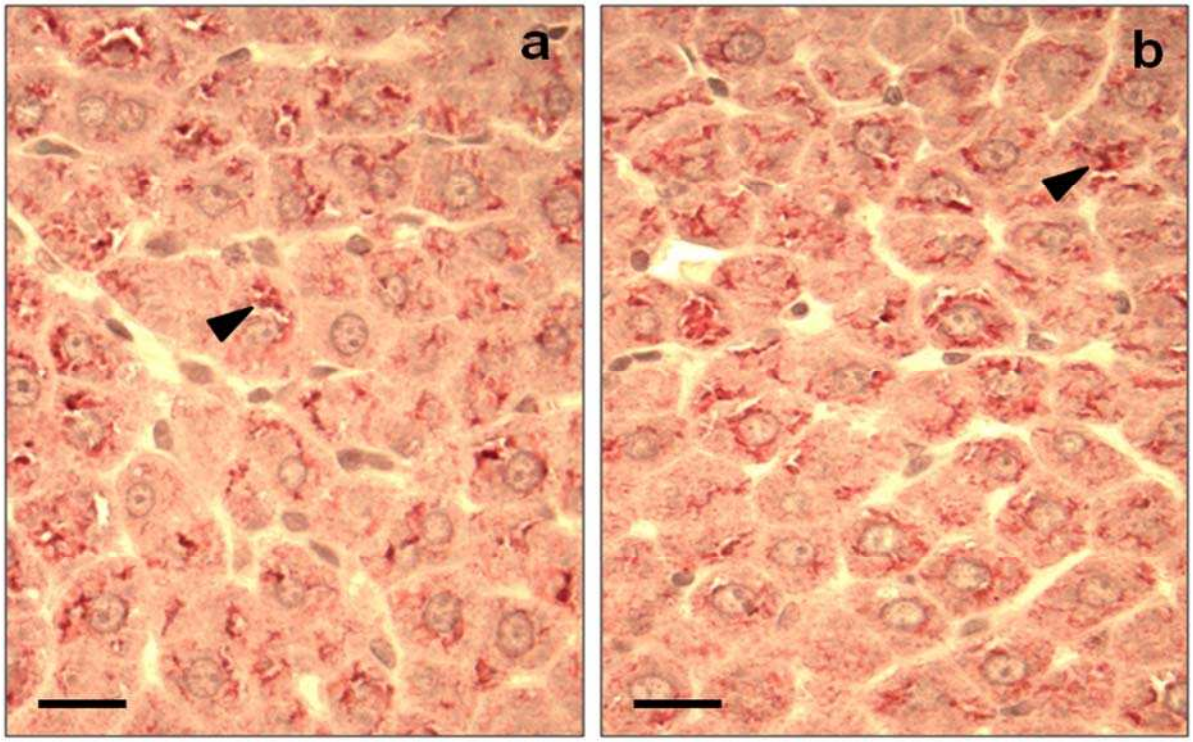

Fig. 1. Representative photomicrographs of the liver from uninfected rats (a, n=10) and rats infected with *Trypanosoma cruzi* (b, n=10). Glycogen cytoplasmic inclusions are indicated by the arrowhead (best carmine method for glycogen; bar = 70μm). Observe the similar glycogen distribution in uninfected and infected animals.

Pancreatic functioning and insulin tolerance

Animals of the IG presented fasted glucose levels that were significantly higher than the CG animals ($p<0.05$). In the OGTT, the IG animals showed high levels of blood glucose at all testing times and abnormal glucose kinetics compared to the CG. For the IG animals, the increase in blood glucose was prolonged and the glucose decay was delayed, only occurring after 90 min (Fig. 2a). The area under the glucose curve was significantly higher in the IG compared to the CG (Fig. 2c).

The levels of blood glucose in the ITT were higher in the IG animals during the test compared to the CG animals, with significant difference after 30 min (Fig. 2b). In addition, the glucose decay rate (KITT) in this test was similar between the groups (Fig. 2d).

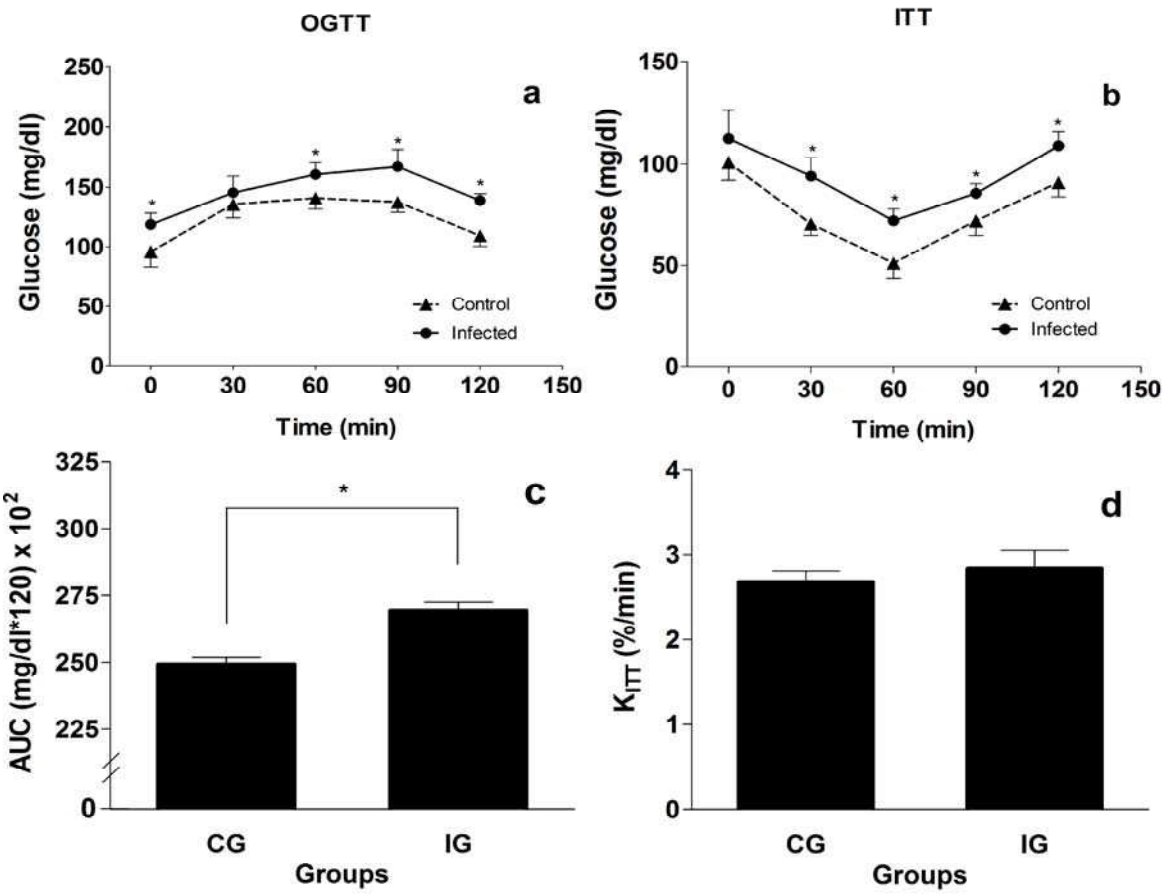

Fig. 2. Blood glucose response after the oral glucose tolerance test (OGTT) and insulin tolerance test (ITT) of rats from control (CG, n=10) and infected (IG, n=10) groups. In the OGTT the area under the glucose curve (AUC) was calculated and in the ITT the glucose decay rate (KITT) was determined. The data are expressed as mean ± SD. The statistical difference between groups was *p < 0.001.

Exercise test protocol and metabolic parameters

Infection with *T. cruzi* impaired exercise tolerance, with a significant reduction in distance traveled and total time to fatigue compared to the CG (Fig. 3a and b). Before exercise, the IG animals presented blood glucose levels that were significantly higher compared to the CG. At this moment in time there was no significant different between the lactate levels in the IG and CG groups. At the point of fatigue, the blood glucose level decreased and the lactate level increased compared to the levels at the beginning of the exercise in both groups. However, no statistical differences were found between the groups for these variables at the point of fatigue (Fig. 3c and d). An inverse and significant

correlation was found between the blood levels of lactate and glucose at the point of fatigue and between lactate and total time to fatigue during the exercise test (Fig. 4a-d) in both groups.

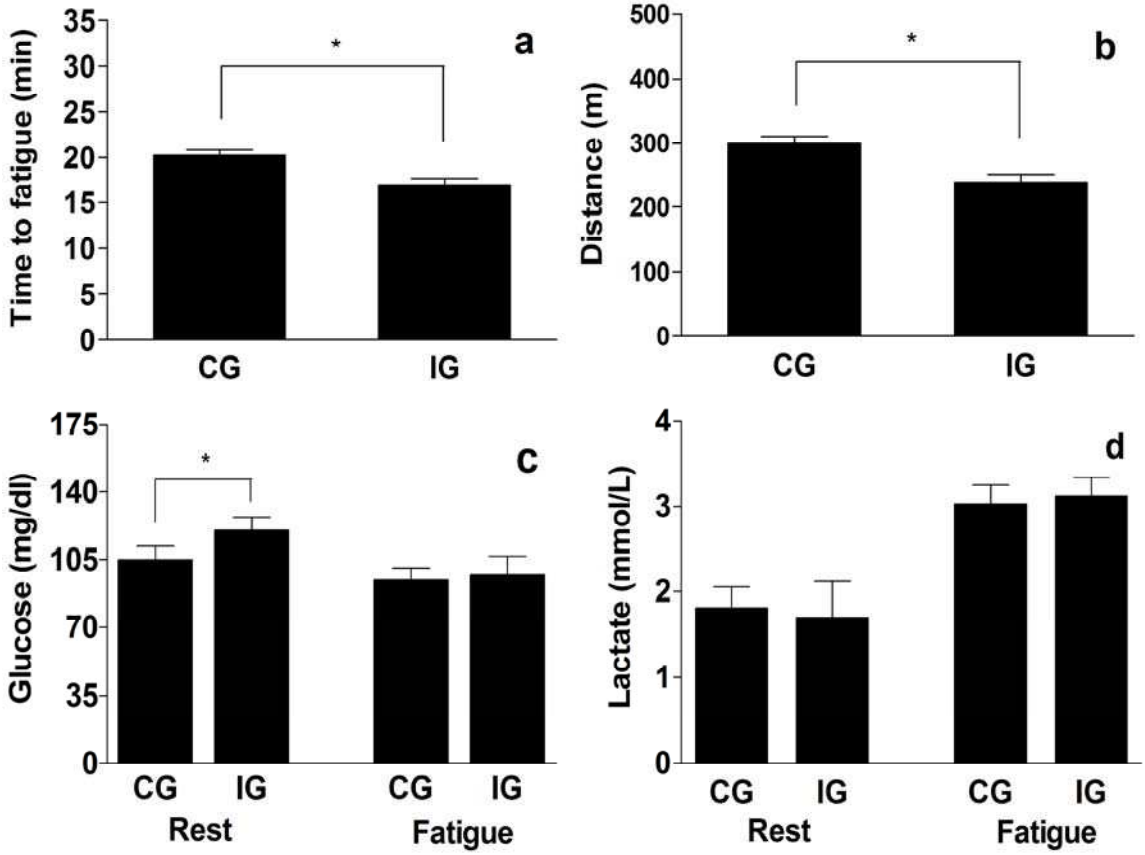

Fig. 3. Spatial, temporal and metabolic parameters of running capacity until the point of fatigue in rats from the control (CG, n=10) and infected (IG, n=10) groups. The data are expressed as mean ± SD. The statistical difference between the groups was *$p < 0.001$.

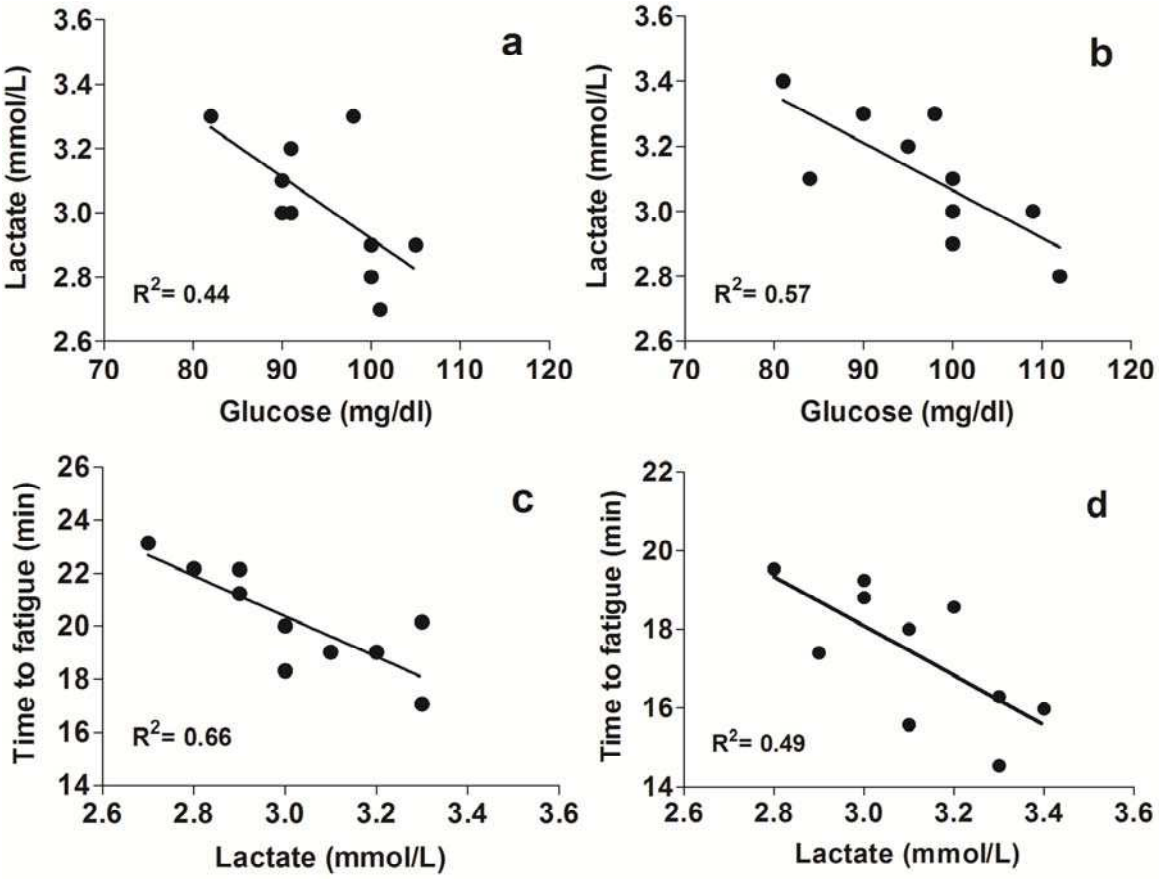

Fig. 4. Correlation between temporal and metabolic parameters of running capacity until the point of fatigue in rats from the control (CG, n=10) and infected (IG, n=10) groups. The correlation data are representative of rats from the control (A and C) and infected (B and D) groups. All correlations were statistically significant ($p < 0.05$).

Histopathological analysis

Histopathological analysis of the heart confirmed the presence of cardiac infection by amastigote forms of *T. cruzi* with cardiomyocyte hypertrophy (Fig. 5b). At the same time pancreatic inflammation was also evident, and vacuolization of acinar cells was observed along with evidence of cell apoptosis in the IG (Fig. 5g-j). In addition, marked inflammatory infiltrates were found in the exocrine pancreas of IG animals with a dominant perivascular, periductal and periacinar distribution (Fig. 5g and j). The infiltration of inflammatory cells into pancreatic islets was scarce (Fig. 5 g,h and j).

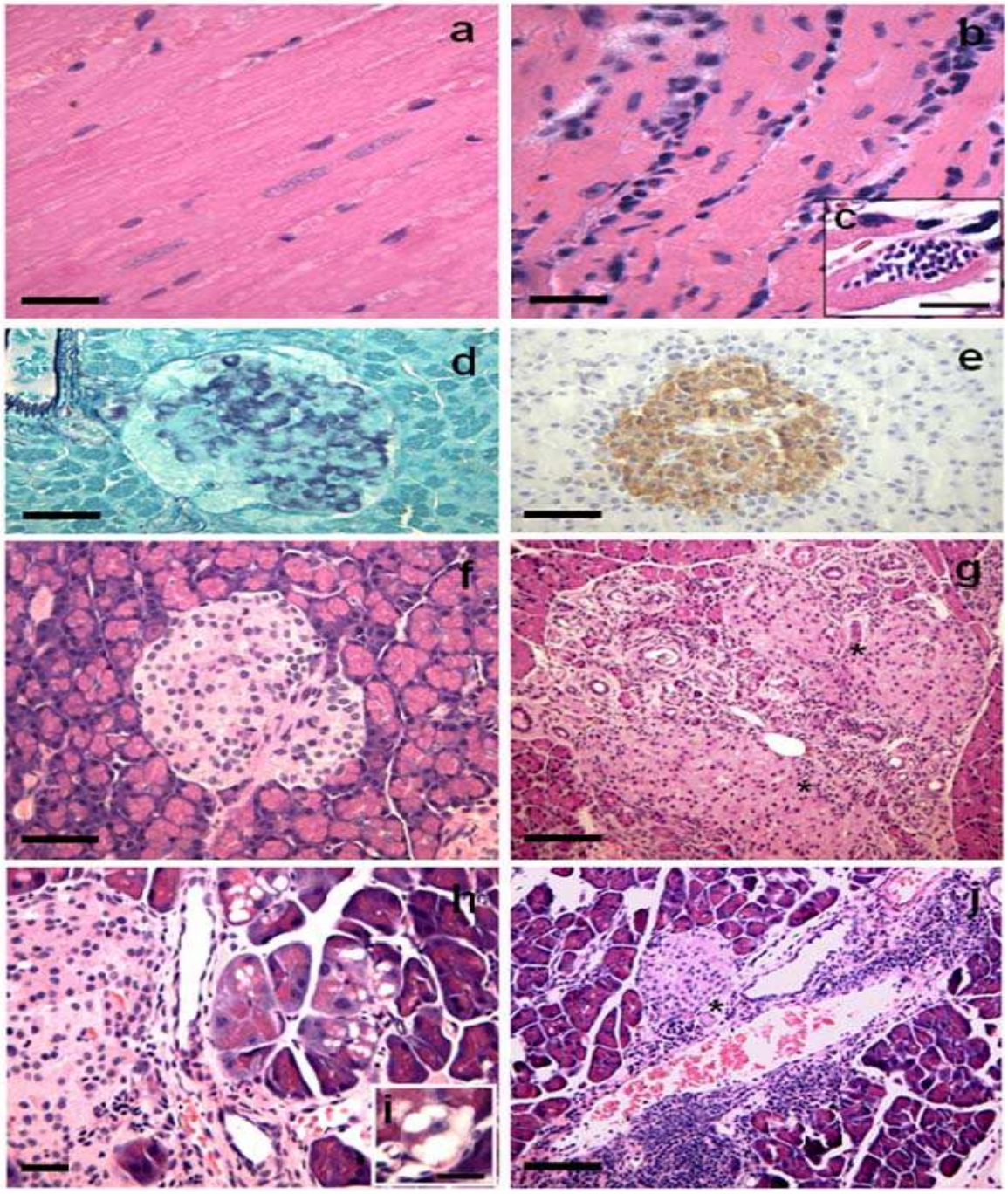

Fig. 5. Representative photomicrographs of the ventricular myocardium and pancreas from uninfected rats (a, d, e and f, n=10) and rats infected with *Trypanosoma cruzi* (b, c, g, h, i and j, n=10). (a) Myocardial longitudinal section showing a well-organized structure and low cellularity. (b) Cardiac myocytes with increased diameters and intense pericellular inflammatory infiltrates (H&E staining, bar = 20 μm). (c) Amastigote forms of *T. cruzi* in the myocyte cytoplasm (H&E staining, bar = 10 μm). The same pattern of β cell labeling is shown in panel d (aldehyde-fuchsin histochemistry, bar = 60 μm) and e (insulin immunocytochemistry, bar = 60 μm). (f) Normal morphology of endocrine (islet) and exocrine pancreas (H&E staining, bar = 60 μm). (g and j) Intense inflammatory infiltrates

and disorganization of the exocrine pancreas and minor inflammatory infiltrates in the pancreatic islets (asterisk) (H&E staining, bar = 100 µm). (h) Vacuolization and hypochromia of acinar cells (H&E staining, bar = 25 µm). (I) Detailed cell vacuolization, suggesting the occurrence of apoptosis (H&E staining, bar = 15 µm).

The number of both MN and PMN cells was significantly higher in IG compared to CG ($p < 0.05$) (Figure 6a). The IG animals also showed significantly higher collagen and protein carbonyl contents compared to CG animals ($p < 0.05$) (Figure 6b and c).

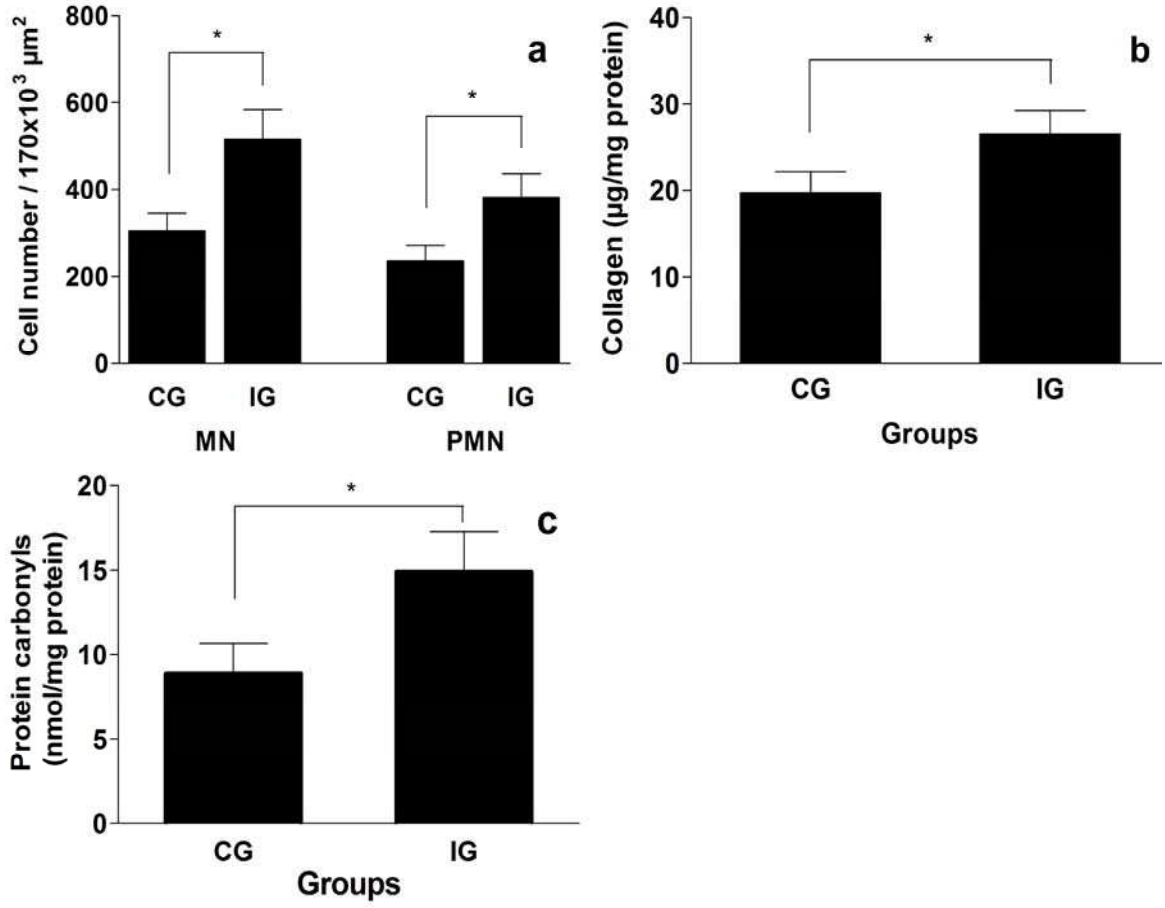

Fig. 6. Analysis of inflammation, collagen and protein oxidation in the pancreas of rats from control (CG, n=10) and infected (IG, n=10) groups. MN, mononuclear cells, PMN, polymorphonuclear cells. The data are expressed as mean ± SD. The statistical difference between the groups was *$p < 0.001$.

Stereology and karyometry

The quantitative morphological parameters are shown in Table 1. No significant differences were found between the groups for all relative and absolute parameters estimated in the stereological analysis. The karyometric variables were significantly reduced in IG animals compared to CG animals ($p < 0.05$).

Table 1. Stereology of the pancreatic tissue and Karyometry of β cell nuclei in rats from control (CG, n=10) and infected (IG, n=10) groups.

Parameters	Control group	Infected group
Vv [islet] (%)	2.920 ± 1.451	2.760 ± 1.370
Vi [µm3]	2022648.264 ± 641182.222	1727643.212 ± 759538.311
Vv [β cell] (%)	64.690 ± 10.950	60.480 ± 9.300
NAC [β cells/µm2]	0.010 ± 0.005	0.008 ± 0.003
NVC [β cells/µm3]	0.043 ± 0.014	0.034 ± 0.010
N [β cell/islet]	69250.763 ± 28165.934	73145.215 ± 36424.107
Nuclei axis (µm)	7.130 ± 0.530	6.460 ± 0.630*
Nuclei area (µm2)	12.770 ± 1.930	10.520 ± 1.990*
Nuclei volume - (µm3)	192.650 ± 44.480	144.790 ± 39.820*

Vv, volume density; NAC, number density per islet area; NVC, number density per islet volume; Vi, islet volume. Data are expressed as mean ± S.D. Statistical difference between groups (*$p < 0.001$).

Discussion

In the present study, infection was induced with the *T. cruzi* Y strain due to its high virulence and capacity to parasitize several organs and tissues. Moreover, this strain has also shown evidence of a similar immune-pathogenic mechanism in humans and rats [24]. Due to the resistance of rats to *T. cruzi*, a high parasite number was used in the inoculum to

induce infection, which was confirmed in all of the IG animals. Our results showed that the inoculum and the consequential *T. cruzi* infection were sufficient to induce a marked dysfunction in glucose kinetics at rest and during exercise and a reduction in exercise tolerance in the IG animals. Interestingly, such alterations occurred in the presence of marked morphological changes in the exocrine pancreas and minimal changes in the endocrine pancreas.

Changes in glucose metabolism in ChD have been reported in human [18,26,35] and animal model of *T. cruzi* infection [34]. Evidence has been found showing that the modifications in body composition are able to alter the insulin response and consequently glucose kinetics [9]. Due to the systemic characteristics of ChD the occurrence of anorexia and weight loss are not unusual [36], which are events that can affect the levels of blood glucose in OGTT and ITT and during exercise. After 9 weeks of infection no significant difference was found in body mass, Lee index, or the volume density of glycogen inclusions in the liver tissue between IG and CG animals, a finding that reduced the influence of body mass and changes in the glycogen stores on the results obtained.

Since the same glucose curves were found in the ITT for both the IG and CG animals, a dysfunction in glucose kinetics does not seem to be related to the peripheral insulin resistance in *T. cruzi* infection, a finding that was reinforced by the similar glucose decay rates (KITT) found in both groups. Insulin resistance cannot be disregarded in the pathogenesis of glucose metabolism dysfunctions in ChD; however, it has been reported that insulin resistance appears to be mainly related to the comorbidities associated with ChD, such as obesity and diabetes mellitus [18,35].

The present study showed for the first time that *T. cruzi* infection affects glucose and lactate metabolism during exercise, leading to a reduction in exercise tolerance. Exercise intolerance has traditionally been related to cardiac dysfunction in chagasic subjects [10,16,17,20]; however, the metabolic mechanisms associated with exercise intolerance remain poorly understood. It is believed that immune-mediated mechanisms and the increase in oxidative stress triggered by *T. cruzi* could be associated with exercise intolerance in ChD. In fact, there is evidence to show that the increased secretions of chemokine MCP-1 induced by *T. cruzi* are related to muscle weakness and reduced exercise capacity in chagasic patients [40]. In addition, previous studies showed that *T. cruzi* infection reduces the activity of antioxidant enzymes and stimulates the production of free radicals, events that cause a dysfunction in the cellular metabolism of energy via the uncoupling of several enzymatic complexes integrated within the electron transport chain

[13,41,42]. However, whether or not these molecular changes are associated with dysfunctions in glucose and lactate metabolism due to *T. cruzi* infection warrants further investigation.

Although no statistical differences were found between the blood glucose and lactate levels at the end of the exercise test, reductions in time to fatigue and the distance traveled during the exercise test were found. In addition, the blood glucose and lactate levels showed an inverse and significant correlation at the end of the exercise test, similar to those observed between lactate and total time to fatigue. These findings suggest that the IG animals presented a higher energetic expenditure and a more active anaerobic metabolism compared to the CG. A lower energetic efficiency due to the increased anaerobic metabolism of glucose is proposed as a mechanism for partially explaining the exercise intolerance in *T. cruzi* infection. This mechanism is not unrealistic considering the possible negative influence of the infection in the electron transport chain and hence in the aerobic process of energy production [13,41,42]. In this context, a previous study showed that chagasic patients had increased levels of anaerobic metabolism that were associated with vascular dysfunction, reduced levels of VO2 max, lactate dehydrogenase, citrate synthase and, consequently, exercise tolerance [23]. Thus, a more glycolytic and less oxidative glucose metabolism is consistent with an increased production of lactate and with the anticipation of fatigue point during a progressive exercise protocol, as used in the present study. However, there is sufficient evidence that the determination of exercise tolerance is multifactorial. Thus, as *T. cruzi* is able to parasitize and damage structures such as peripheral nerves and skeletal muscles, equally important elements in determining the exercise tolerance [16,17,23,40], we cannot attribute the results exclusively to the metabolic changes. In this context, the weak correlation between glucose and lactate levels and time to fatigue indicates that other organs and tissues should be investigated to improve the knowledge about the pathophysiological mechanism related to exercise intolerance in Chagas' disease.

Histopathological evidence of pancreatitis was observed in the IG animals. Based on the stereological analysis of the IG, morphological changes in the exocrine pancreas were more pronounced compared to those in the endocrine pancreas. However, the karyometric parameters of the β cells in the IG animals were markedly reduced compared to the CG animals. From a morphological point of view, in the case of pancreatitis caused by *T. cruzi* several other hypotheses can be used in an attempt to explain the dysfunction in glucose kinetics, such as hypoinsulinemia caused by insulitis, chronic inflammation with pancreatic

fibrosis and microvascular damage, and parasympathetic denervation of pancreatic islets with the predominance of sympathetic stimuli [7,26,34,35]. Similar mechanisms have been described in other severe protozoan infections, such as malaria [6,34]. Some studies reported that hypoinsulinemia caused by the direct disruption of β cells by *T. cruzi* may be an important mechanism involved in the dysfunction of glucose metabolism, especially hyperglycemia [18,34]. This mechanism was not supported in the present study because of the number of β cells in the pancreatic islets of IG animals compared to CG animals was not reduced. However, possible functional changes rather than structural defect in insulin-producing cells cannot be excluded. Thus, it is possible that the occurrence of hypoinsulinemia in *T. cruzi* infection was due to a reduction in the glucose-induced release of insulin by β cells and a failure in the counter-regulation of hypoglycemia dependent on parasympathetic stimuli [18,26,34]. Furthermore, due to the high content of protein carbonyl in pancreatic tissue, we cannot rule out the possibility of an endocrine pancreatic dysfunction secondary to oxidative inhibition of receptors or other proteins that participate in cell signaling pathways. Although this mechanism is possible, it must still be proven. In fact, as an abnormal glucose curve in the OGTT was observed in the present study, it is possible that functional changes in β cells could be directly linked to a dysfunction in glucose metabolism at rest rather than peripheral insulin resistance. As the levels of insulin were not investigated these functional changes cannot be determined, which was the main limitation of the present study.

Although many hypotheses have been proposed, the physiopathological mechanisms of glucose metabolism dysfunctions in ChD remain poorly understood. This situation is unfortunately worsened by the shortage of studies on the metabolic repercussions of *T. cruzi* infection related to organs other than the heart and gut. Thus, additional studies should be performed to better clarify the biochemical and molecular basis of glucose metabolism dysfunctions at rest and during exercise in *T. cruzi* infection. Taken together, the data obtained from this study allow us to conclude that *T. cruzi* infection impaired glucose metabolism at rest and during exercise in rats, which could constitute an additional mechanism underlying the exercise intolerance encountered in ChD. It is important to emphasize the fact that as these metabolic changes were observed in the absence of pronounced morphological changes of the pancreatic islets, further studies are required to better characterize the relationship between the endocrine pancreas and glucose metabolism at rest and during exercise in ChD. Finally, the results were important to

indicate the need to extend investigations to other organs, suggesting that the pancreas may not be exclusively involved in the metabolic abnormalities observed in *T. cruzi* infection.

Acknowledgments

Research supported by FAPEMIG (PRONEX). Rômulo D. Novaes was recipient of Ph.D. scholarship from CAPES.

References

1. L.L. Bernardis, B.D. Petterson, Correlation between "Lee index" and carcass fat content in weanling and adult female rats with hypothalamic lesions. J. Endocrinol. 40 (1968) 527-528.
2. M. Bradford, A rapid and sensitive method for quantitation of microgram quantities of protein utilizing the principle of protein-dye-binding. Anal. Biochem. 72 (1976) 248-254.
3. Z. Brener, Therapeutic activity and criterion of cure on mice experimentally infected with Trypanosoma cruzi. Rev. Inst. Med. Trop. São Paulo 4 (1962) 389-396.
4. A. Biolo, A.L. Ribeiro, N. Clausell, Chagas cardiomyopathy-where do we stand after a hundred years? Prog. Cardiovasc. Dis. 52 (2010) 300-316.
5. I.S. Caldas, A. Talvani, S. Caldas, C.M. Carneiro, M. Lana, P.M.M. Guedes, M.T. Bahia, Benznidazole therapy during acute phase of Chagas disease reduces parasite load but does not prevent chronic cardiac lesions. Parasitol. Res. 103 (2008) 413-421.
6. I.A. Clark, F.M. Al Yaman, L.S. Jacobson, The biological basis of malarial disease. Int. J. Parasitol. 27 (1997) 1237-1249
7. C.E.P. Corbett, L.H.G. Scremin, R.A. Lombardi, J.J. Gama-Rodrigues, M. Okumura, Pancreatic lesions in acute experimental chagas' disease. Rev. Hosp. Clín. Fac. Med. São Paulo 57 (2002) 63-66.
8. W. Creutzfeldt, R. Ebert, M. Nauck, F. Stöckmann, Disturbances of the entero-insular axis. Scand. J. Gastroenterol. 82 (1983) 111-119.
9. H.A. Durham, G.E. Truett, Development of insulin resistance and hyperphagia in Zucker fatty rats. Am. J. Physiol. Regul. Integr. Comp. Physiol. 290 (2006) 652-658.

10. L.Jr. Gallo, J.A. Neto, J.C. Manco, A. Rassi, D.S. Amorim, Abnormal heart rate responses during exercise in patients with Chagas' disease. Cardiology 60 (1975) 147-62.
11. G. Gomori, Aldehyde fuchsin: A new stain for elastic tissue. Am. J. Clin. Pathol. 20 (1950) 665-666.
12. H.J. Gundersen, T.F. Bendtsen, L. Korbo, N. Marcussen, A. Moller, K. Nielsen, J.R. Nyengaard, B. Pakkenberg, F.B. Sorensen, A. Verterby, Some new, simple and efficient stereological methods and their use in pathological research and diagnosis. APMIS 96 (1988) 379-394.
13. S. Gupta, J. Wen, N.J. Garg, Oxidative stress in Chagas disease. Interdiscip. Perspect. Infect. Dis. ID190354 (2009) 1-8.
14. L.G. Koch, S.L. Britton, Artificial selection for intrinsic aerobic endurance running capacity in rats. Physiol. Genomics 5 (2001) 45-52.
15. A.C. Lacerda, U. Marubayashi, C.H. Balthazar, C.C. Coimbra, Evidence that brain nitric oxide inhibition increases metabolic cost of exercise, reducing running performance in rats. Neurosci. Lett. 393 (2006) 260-263.
16. M.M.O. Lima, M.C. Pereira, M.O.C. Rocha, F.R. Beloti, M.C.N. Alencar, A.L.P. Ribeiro, Left ventricular diastolic function and exercise capacity in patients with Chagas cardiomyopathy. Echocardiography 27 (2010a) 519-524.
17. M.M.O. Lima, M.O.C. Rocha, M.C.P. Nunes, L. Sousa, H.S. Costa, M.C.N. Alencar, R.R. Britto, A.L.P. Ribeiro, A randomized trial of the effects of exercise training in Chagas cardiomyopathy. Eur. J. Heart Fail. 12 (2010b) 866-873.
18. R.G. Long, R.H. Albuquerque, A. Prata, A.J. Barnes, T.E. Adrian, N.D. Christofides, S.R. Bloom, Response of plasma pancreatic and gastrointestinal hormones and growth hormone to oral and intravenous glucose and insulin hypoglycaemia in Chagas's disease. Gut 21 (1980) 772-777.
19. A. López-De León, M. Rojkind, A simple micromethod for collagen and total protein determination in formalin-fixed paraffin-embedded sections. Histochem. Cytochem. 33 (1985) 737-743.
20. C. Mady, B.M. Ianni, E. Arteaga, V.M.C. Salemi, C.C. Frimm, Maximal functional capacity in patients with chagas' cardiomyopathy without congestive heart failure. J. Card. Fail. 3 (2000) 220-224.

21. C.A. Mandarim-de-Lacerda, Stereological tools in biomedical research. An. Acad. Bras. Ciênc. 75 (2003) 469-486.
22. P.M. Martinelli, E.R.S. Camargos, A.A. Azevedo, E. Chiari, G. Morel, C.R.S. Machado, Cardiac NGF and GDNF expression during *Trypanosoma cruzi* infection in rats. Auton. Neurosci. 130 (2006) 32-40.
23. M. Montes de Oca, S.H. Torres, J.G. Loyo, F. Vazquez, N. Hernández, B. Anchustegui, J.J. Puigbó, Exercise performance and skeletal muscles in patients with advanced Chagas disease. Chest 125 (2004) 1306-1314.
24. S.A. Morris, H.B. Tanowitz, M. Wittner, J.P. Bilezikian, Pathophysiological insights into the cardiomyopathy of Chagas' disease. Circulation 82 (1990)1900-1909.
25. R.D. Novaes, R.V. Gonçalves, D.C. Marques, M.C. Cupertino, M.C. Peluzio, J.P. Leite, I.R. Maldonado, Effect of bark extract of *Bathysa cuspidata* on hepatic oxidative damage and blood glucose kinetics in rats exposed to paraquat. Toxicol. Pathol. 40 (2012) 62-70.
26. L.C.M. Oliveira, Y. Juliano, N.F. Novo, M.M. Neves, Blood glucose and insulin response to intravenous glucose by patients with chronic Chagas' disease and alcoholism. Braz. J. Med. Biol. Res. 26 (1993) 1187-1190.
27. P. Pushparaj, C.H. Tan, B.K.H. Tan, Effects of *Averrhoa bilimbi* leaf extract on blood glucose and lipids in streptozotocin-diabetic rats. J. Ethnopharmacol. 72 (2000) 69-76.
28. A. Rassi-Jr, A. Rassi, J.A. Marin-Neto, Chagas disease. Lancet 375 (2010) 1388-1402.
29. P.G. Reeves, F.H. Nielsen, G.C. Fahey Jr, AIN-93 purified diets for laboratory rodents: final report of the American Institute of Nutrition ad hoc writing committee on the reformulation of the AIN-76A rodent diet. J. Nutr. 123 (1993) 1939-1951.
30. A. Rocha, L.C. de Oliveira, R.S. Alves, E.R. Lopes, Pancreatic neuronal loss in chronic Chagas' disease patients. Rev. Soc. Bras. Med. Trop. 31 (1998) 43-49.
31. M.A. Sala, M.C. Komesu, R.A. Lopes, C.G. Maia, Karyometric study of basal cell carcinoma. Braz. Dent. J. 5 (1994) 11-4.
32. J.C. Saldanha, V.M. Santos, M.A. Reis, D.F. Cunha, V.P.A. Teixeira, Morphologic and morphometric evaluation of pancreatic islets in chronic Chagas' disease. Rev. Hosp. Clin. Fac. Med. São Paulo 56 (2001) 131-138.
33. V.M. Santos, M.A. Lima, M. Cabrine-Santos, D.E. Márquez, M.G. Reis, G.A. Pereira, E. Lages-Silva, L.E. Ramírez, Pancreatic hepatocytes in hamsters (*Mesocricetus auratus*) infected with *Trypanosoma cruzi*. Exp. Parasitol. 100 (2002) 103-111.

34. V.M. Santos, M.A. Lima, M. Cabrine-Santos, D.S. Marquez, G.A. Pereira, E. Lages-Silva, L.E. Ramírez, Functional and histopathological study of the pancreas in hamsters (*Mesocricetus auratus*) infected and reinfected with *Trypanosoma cruzi*. Parasitol. Res. 94 (2004) 125-133.
35. V.M. Santos, S.F.C. Cunha, V.P. Teixeira, J.P. Monteiro, J.A. Santos, T.A. Santos, L.A. Santos, D.F. Cunha, Frequency of diabetes mellitus and hyperglycemia in chagasic and non chagasic women. Rev. Soc. Bras. Med. Trop. 32 (1999) 489-496.
36. C. Schebeleski-Soares, R.C. Occhi, S.M. Franzói-de-Moraes, M.M.D. Oliveira, F.N. Almeida, M.J.O. Toledo, S.M. Araújo, Preinfection aerobic treadmill training improves resistance against *Trypanosoma cruzi* infection in mice. Appl. Physiol. Nutr. Metab. 34 (2009) 1-8.
37. W.M. Sherman, Metabolism of sugars and physical performance. Am. J. Clin. Nutr. 62 (1995) 228S-241S.
38. R.S. Sohal, S. Agarwal, A. Dubey, W.C. Orr, Protein oxidative damage is associated with life expectancy of houseflies. Proc. Natl. Acad. Sci. 90 (1993) 7255-7259.
39. L.A. Sternberger, The unlabelled antibody peroxidase antiperoxidase (PAP) method, In: S. Cohen, R.T. McClusky (Eds.), Immunocytochemistry, second ed., John Wiley and Sons, New York, (1979), pp. 104-169.
40. L. Sousa, F.A. Botoni, R.R. Britto, M.O.C. Rocha, A.L. Teixeira-Jr, M.M. Teixeira, A.M. Reis, B.M.R. Oliveira, A.L. Ribeiro, Six-minute walk test in Chagas cardiomyopathy. Int. J. Cardiol. 125 (2008) 139-141.
41. J. Wen, M. Dhiman, E.B. Whorton, N.J. Garg, Tissue-specific oxidative imbalance and mitochondrial dysfunction during *Trypanosoma cruzi* infection in mice. Microbes Infect. 10 (2008) 1201-1209.
42. J. Wen, N. Garg, Oxidative modification of mitochondrial respiratory complexes in response to the stress of *Trypanosoma cruzi* infection. Free Radic. Biol. Med. 37 (2004) 2072-2081.

Artigo 3

Trypanosoma cruzi infection induces morphological reorganization of the myocardium parenchyma and stroma and modifies the mechanical properties of atrial and ventricular cardiomyocytes in rats

Rômulo D. Novaes[a], Arlete R. Penitente[a], Reggiani V. Gonçalves[b], André Talvani[c], Maria C.G. Peluzio[d], Clóvis A. Neves[a], Antônio J. Natalie, and Izabel R.S.C. Maldonado[a]

[a]Department of General Biology, Federal University of Viçosa, Viçosa, MG, Brazil

[b]Department of Morphology, Federal University of Pelotas, Pelotas, RS, Brazil

[c]Department of Biological Sciences and NUPEB, Federal University of Ouro Preto, Ouro Preto, MG, Brazil

[d]Department of Nutrition and Health, Federal University of Viçosa, MG, Brazil

[e]Department of Physical Education, Federal University of Viçosa, Viçosa, MG, Brazil

Correspondence: Izabel R.S.C Maldonado, Federal University of Viçosa, Department of Physical Education. Av. Peter Henry Rolfs, s/nº, Zip code: 35.570-000. Viçosa-MG, Brasil. Phone: +55 31 3899-4390. Fax: +55 31 3899-2249. E-mail: irscosta@ufv.br

Abstract

This study investigates morphofunctional adaptations of the heart stroma and parenchyma in rats that are chronically infected with *Trypanosoma cruzi*. Four-month-old male Wistar rats were randomized into control (n= 14) and infected (n= 14) groups. Infected animals were inoculated with *T. cruzi* Y strain. After nine weeks the animals were euthanized and the right atrium (RA) and left ventricle (LV) were removed for biochemical, stereological and cardiomyocyte mechanical analyses. Infected animals presented cardiomyocyte atrophy, cytoplasmic fragmentation, myocardial fibrosis and necrosis. For these animals, the total volume, length, surface area and cross-sectional area of cardiomyocytes were significantly reduced and the total interstitial and collagen volumes were significantly increased in the RA and LV compared to the controls. The total volume and length of blood vessels were significantly increased in the LV, and the total blood vessel surface area was significantly higher in the RA of infected animals. RA and LV cardiomyocytes from infected animals exhibited a significant reduction in cell shortening (43.02% and 24.98%, respectively), prolongation of the time to the peak of contraction (17.09%) and the time to half relaxation (23.68%) compared to non-infected animals. Lipid hydroperoxides, but not mineral concentrations, were significantly increased in the RA and LV from infected animals, showing an inverse correlation with cell shortening. *T. cruzi* infection induces global structural remodeling of the RA and LV in rats. This remodeling coexists with cardiomyocyte contractility dysfunction, which is possibly related to the abnormal organization of the myocardial stroma and increased cellular lipid peroxidation.

Keywords: Cardiac myocytes, Chagas' disease, pathology, extracellular matrix, oxidative stress, X-ray spectroscopy.

Introduction

Chagas' disease (American Trypanosomiasis) is caused by the hemoflagellate protozoan parasite *Trypanosoma cruzi*. This parasite infects nearly 10 million people worldwide and remains a leading cause of chronic heart failure in Central and South America (Santos et al. 2012) despite dramatic progress in transmission control (Lima et al. 2010a). Thousands of patients die every year, mainly due to dilated cardiomyopathy, congestive heart failure, dysrhythmias and thromboembolic events that occur in approximately 30% of infected subjects (Marin-Neto et al. 2007; Rassi-Jr et al. 2010). Owing to population migration, Chagas' disease also has the potential to become a health problem in non-endemic countries (Guerri-Guttemberg et al. 2008; Lima et al. 2010a).

Although there is evidence that *T. cruzi* is able to spread and infect several organs, such as the gonads, kidney, liver and pancreas in humans and animals, the cardiac form of the disease is the more severe and disabling (Rassi-Jr et al. 2010; Rossi et al. 2010). Due to the intracellular parasite replication, differentiation and cell evasion that occur during the acute phase of *T. cruzi* infection, the parasite triggers a destructive process in the myocardium. It has been suggested that this process is associated with an imbalance in the myocardial oxidative status, in which there is an increase in lipid and protein oxidation that causes progressive deterioration of the cardiomyocyte structure and function, and eventually, leads to cell death (Wen et al. 2004; Wen and Garg, 2004; Gupta et al. 2009a,b). In parallel to myocardium destruction there is a reaction to repair the heart parenchyma and stroma, which reduces the progression of the cardiac lesions, reducing the severity of the infection (Biolo et al. 2010; Rassi-Jr et al. 2010). The heart failure observed in severe cases of the disease develops gradually during *T. cruzi* infection, when destructive events outweigh the reparative myocardial events (Marin-Neto et al. 2007; Rossi et al. 2010).

During the transition from the acute to the chronic phase of *T. cruzi* infection, there is a progressive morphological and functional reorganization of the heart (Lima et al. 2010a,b; Rossi et al. 2010). Traditionally, the evidence of myocardium structural remodeling induced by *T. cruzi* is mainly based on qualitative or semi-quantitative studies (Morris et al. 1990; Higuchi et al. 1993, 1999; Rossi, 1998; Biolo et al. 2010). Moreover, most of the histo-quantitative data are described as relative values related to a two-dimensional (2D) reference space. To the best of our knowledge, the basic characteristics of the myocardial morphological reorganization in a three-dimensional (3D) space remain an unresolved issue in *T. cruzi* infection. Therefore, understanding the extent of cardiac damage in

Chagas' cardiomyopathy (ChC) is essential for the design of rational intervention strategies.

In addition to the morphological remodeling of the heart in ChC, pathological changes in cardiac function are also commonly seen. Electrical changes of the sinus rhythm, conduction blocks of the action potential and atrial and ventricular arrhythmias have been widely described (Marin-Neto et al. 2007; Biolo et al. 2010). Moreover, mechanical and hemodynamic abnormalities, such as reduced end-diastolic volume, different strengths of muscle contractions, and altered heart rate and cardiac output, are also involved in cardiac dysfunction and contribute to the increased risk of death in *T. cruzi* infection (Lima et al. 2010a,b; Rassi-Jr et al. 2010; Santos et al. 2012). However, the biochemical and cellular basis of ChC remains poorly understood.

Thus, this study used a stereological approach and cell isolation to investigate the morphofunctional adaptations of the heart stroma and parenchyma in the chronic phase of *T. cruzi* infection. Considering the relationship between cardiac structure and function, this study investigates the hypothesis that structural myocardial remodeling coexists with changes in oxidative status of the myocardium and pathological adaptations of the cardiomyocytes mechanical properties.

Materials and Methods

Animals and infection

Four-month-old male Wistar rats were provided with rodent chow and water *ad libitum* and maintained in animal facilities with a controlled environment (temperature at 22 ± 3ºC, humidity at 60-70% and 12 hour light/dark inverted cycles). Animals were randomly divided into control (CG, n= 14) and infected (IG, n= 14) groups. Animals from the IG were inoculated intraperitoneally with the *T. cruzi* Y strain (300,000 trypomastigotes⁄50g body weight) (Martinelli et al. 2006) contained in 700µl of infected blood from a mouse that had been diluted in 0.9% saline solution. Infection was confirmed four days post-inoculation by the presence of trypomastigotes in peripheral blood collected from the rat's tail as described by Brener (1962). Nine weeks after inoculation the animals were euthanized under anesthesia and the hearts were removed for stereological and contractile function analyses. All experimental procedures were conducted in accordance with the

Brazilian College of Animal Experimentation and approved by the Animal Research Ethics Commission of the Federal University of Viçosa, Brazil (protocol 30/2009).

Sample size and tissue processing

The hearts from five animals per group were removed for stereological analysis. The sample size for this analysis was determined considering the probability P=1/2 to increase or decrease of the variables of interest. Thus, considering the significance level α=0.05, the minimal significant number of animals used in the statistical analysis was P=(1/2)events; so, if n=5, P=(1/2)5 or P=0.03; thus, P<0.05 (Cruz-Orive and Weibel, 1990).

The right atrium (RA) and the left ventricle (LV) were dissected and the volumes were determined using the submersion method described by Scherle (1970). The LV volume was determined, including the inter-ventricular septum. The RA and LV were placed into histological fixative for 48 hours (freshly prepared 10% w/v formaldehyde in 0.1M phosphate buffer pH 7.2). The fragments of the RA and LV were obtained through the *orientador* method for stereological study (Mandarim-de-Lacerda, 2003). These fragments were dehydrated in ethanol, cleared in xylol and embedded in paraffin. Blocks were cut into 4µm-thick thick histological sections stained with hematoxylin-eosin (H&E), 4',6-diamidino-2-phenylindole (DAPI) and Phalloidin, and mounted on histology slides. To avoid repeated analysis of the same histological area, sections were evaluated in semi-series, using 1 out of every 20 sections. The slides were visualized and the images captured using a light microscope (Olympus BX-60®, Tóquio, Japan) connected to a digital camera (Olympus QColor-3®, Tokyo, Japan). Sections stained with DAPI and Phalloidin were visualized using the epifluorescence mode of the same microscope.

Tissue shrinkage

The processing of biological tissues for microscopy often leads to tissue shrinkage, especially when embedded in paraffin. In order to avoid false estimations of the absolute stereological parameters, tissue shrinkage was calculated. Two small tissue fragments with known volumes (Scherle, 1970) from each animal were carefully embedded in paraffin. The embedded samples were totally cut with a microtome advance of 5µm and every 25th section was mounted on a histology slide. The tissue block volumes were microscopically determined using the Cavalieri's principle (Dorph-Petersen et al. 2001), and this volume

was compared to the original volume of the tissue blocks before embedding. The global shrinkage of cardiac tissue was 21% and the stereological estimates were corrected using this index.

Estimation of absolute stereological parameters, cross-sectional area of cardiomyocytes and diffusion distance

All of the stereological analysis was performed according Brüel et al. (2005). The volume density occupied by cardiomyocytes (Vv[*cmy*], %), interstitium (Vv[*int*], %) and blood vessels (Vv[bvs], %) in the RA and LV were estimated by point counting according to the following formula:

$$Vv[structure\ /\ RA;LV] = \frac{\sum P[structure]}{\sum Pt};$$

(1)

where Σ*P*[structure] is the number of points that hit the interest structure and Σ*Pt* denotes the total test points. For these analyses, a test system of 42 points was used in an unbiased two-dimensional test area (*At*) of 1.38x104µm2 at tissue level.

The length density of the cardiomyocytes (Lv[cmy], mm^{-2}) and blood vessels (Lv[bvs], mm^{-2}) in the RA and LV, were estimated as follows:

$$Lv[structure\ /\ RA;LV] = 2 \times \frac{\sum Q^{-}[structure]}{\sum P[RA;LV]} \times \frac{Pt}{At};$$

(2)

where Σ*Q*-[*structure*] denotes the total number of interest structure profiles counted in the *At*, and Σ*P*[*RA; LV*] is the total number of points hitting the RA and LV (the reference space) (Brüel et al. 2005).

The surface area density of the cardiomyocytes (Sv[cmy], mm^{-1}) and blood vessels (Sv[bvs], mm^{-1}) in the RA and LV, were estimated using the following equation:

$$Sv[structure\ /\ RA;LV] = 2 \times \frac{\sum I[structure]}{\sum P[structure]} \times \frac{Pt}{l};$$

(3)

where Σ*I*[*structure*] denotes the total number of intersections between the test lines (here 21) and the surface area of the structure of interest, and l is the length of a test line.

The total volume of cardiomyocytes (V[*cmy*], mm^3), interstitium (V[*int*], mm^3) and blood vessels (V[bvs], mm^3); the total length of cardiomyocytes (L[*cmy*], km) and blood

vessels (L[*bvs*], km); and the total surface area of cardiomyocytes (S[cmy], m^2) and blood vessels (S[bvs], m^2) were estimated by multiplying the relative parameters of density by RA and LV volume.

The mean diffusion distance from capillary to tissue (□[bvs], μm^2), was obtained from equation 4:

$$\text{f}[bvs\ /\ \text{RA; LV}] = \sqrt{\frac{1}{\pi \times \text{Lv}[bvs]}};$$

(4)

The mean cross-sectional area of cardiomyocytes (ā[cmy], μm^2) was calculated as follows:

$$\text{a}[cmy] = \frac{\text{Vv}[cmy]}{\text{Lv}[cmy]};$$

(5)

For all of these analyses, sixty microscopic fields (magnification x400) in sections stained with H&E were randomly sampled and a total of $8.27\times10^5\mu m^2$ of myocardium area was analyzed for each group.

Fibrosis and inflammation

Heart fibrosis was evaluated in 4µm-thick thick histological sections stained with Sirius red dye (Sirius red F3B, Mobay Chemical Co., Union, New Jersey, USA), which marks collagen fibers for observation under a polarizing microscope (Junqueira et al. 1979). The distribution of collagen was analyzed using a segmentation function of the image analysis software Image Pro-Plus 4.5® (Media Cybernetcs, Silver Spring, MD, USA) based on the birefringence properties of the collagen fibrils under polarized light. After image segmentation, the volume density (Vv[*col*], %) and total volume of the myocardium occupied by collagen fibers (V[*col*], µm3) were determined using equation 1 and the RA and LV volumes. In this analysis, sixty microscopic fields were investigated (magnification ×200) by random sampling, and a total myocardium area of $3.34\times10^6\mu m^2$ was analyzed for each group.

The intensity of heart inflammatory process was investigated in sections stained with H&E by the relationship between the mononuclear (MN) and polimorphonuclear (PMN) cell numbers observed in the myocardium from control and infected animals. The tissue

cellularity was evaluated by counting the number of nuclei at ×1000 magnification across sixty random microscopic fields in a total myocardium area of $2.04\times10^5\mu m^2$ for each group (Gundersen et al. 1988). Cardiomyocyte nuclei were excluded from this count. All morphological analysis was performed using the image analysis software Image Pro-Plus 4.5® (Media Cybernetcs, Silver Spring, MD, USA).

Cardiomyocytes isolation and contractile function

At euthanasia, the hearts of nine animals from each group were rapidly removed and the extraneous tissue was dissected away. The hearts were mounted onto a Langendorff perfusion apparatus for the isolation of myocytes using a collagenase-protease dispersion technique as previously described (Natali et al. 2002). Briefly, the heart was perfused for 10-15 min with a solution containing 1mg/ml of collagenase type II (Worthington, USA). Ventricular and atrial cardiomyocyte cells were isolated by mechanical titration over 5 minutes at 37ºC, with single cells separated from the non-dispersed tissue by filtration. Only calcium-tolerant, quiescent, rod-shaped cardiomyocytes showing clear cross striations were studied. The isolated cardiomyocytes were used within 4 h of isolation.

Cellular contractile function was evaluated as described by Natali et al. (2002). Briefly, isolated cells were placed in a chamber with a glass coverslip base mounted on the stage of an inverted-type phase contrast video microscope (Eclipse-TS100®, Nikon, Japan). The chamber was perfused with Tyrode's solution at room temperature (≈ 28ºC). Myocytes were stimulated via platinum bath electrodes with voltage pulses of 5ms duration and an intensity of 20V at 1Hz. Cells were visualized on a PC monitor with an NTSC camera (Myo-Cam CCD100V®, Ionoptix, Milton, MA, USA) set in scanning mode. This image was used to measure cell shortening (index of contractile function) in response to electrical stimulation, using a video motion edge detection system (Ionoptix, Milton, MA, USA). The cell image was sampled at 240Hz and cell shortening was calculated from the output of the edge detector using an IonWizard A/D converter (Ionoptix, Milton, MA, USA). 8 to 16 consecutive contractions were averaged and cell shortening (expressed as percentage of resting cell length), the time to the shortening peak and the time to half-relaxation were calculated (Roman-Campos et al. 2009).

Mineral microanalysis and lipid peroxidation

The mineral content in heart tissue was investigated by Energy Dispersive X-ray Spectroscopy (EDS) using a scanning electron microscope (Leo 1430VP®, Carl Zeiss, Jena, Thuringia, Germany) with an attached x-ray detector system (Tracor TN5502, Middleton, WI, USA). Small RA and LV pieces from each animal that had not been used for the stereological analysis were dissected, and three other fragments were obtained so that each one represented a different region of the myocardium: sub-epicardial, central and sub-endocardial. These fragments were dehydrated in ethanol, submitted to critical point drying (CPD 030®, Bal-tec, Witten, North Rhine-Westphalia, Germany) and coated with a thin film of evaporated carbon (Quorum Q150 T®, East Grinstead, West Sussex, England, UK). The EDS microanalysis was performed at x800 magnification, with an accelerating voltage of 20kV and a working distance of 19 mm. The proportion of the elements carbon (C), nitrogen (N), oxygen (O), potassium (K), phosphorus (P), sodium (Na), calcium (Ca) and magnesium (Mg) were measured by EDS and expressed as a mean value for all of the myocardium regions analyzed.

After enzymatic digestion, aliquots of the RA and LV from each heart used for cardiomyocyte isolation were homogenized in phosphate buffered saline (PBS) and centrifuged at 5ºC. The supernatant was used to determine the lipid hydroperoxide tissue levels using a standardized methodology (Nourooz-Zadeh et al. 1994). Lipid hydroperoxide levels were normalized by the tissue content of total protein measured using the Bradford assay (Bradford, 1976).

Statistical analysis

Data are presented as means and standard deviations (mean ± S.D). Normal distribution of data was verified using the Kolmogorov-Smirnov test. The coefficient of variation (CV) was calculated to investigate the homogeneity in the distribution of animal body mass. The observed total variation (CVtot) and the coefficient of error of the stereological procedure (CEmet) were estimated. From CVtot and CEmet, the biological variation (CVbio) was calculated as follows (Brüel et al. 2005): $CVbio = \sqrt{CVtot^2 - CEbio^2}$. The CE's from the various stereological estimators used are within acceptable limits (Table 1). Biometric, biochemical and cell contractile function data were compared using the student t-test.

Stereological data were compared using the Mann-Whitney U test. A probability of $P < 0.05$ was considered statistically significant.

Table 1 Estimates of coefficients of variation for the stereological parameters

Parameter	Right atrium / Left ventricle		
	***CV*tot**	***CV*bio**	***CE*met**
V[cmy]	0.09 / 0.12	0.09 / 0.11	0.03 / 0.04
V[int]	0.17 / 0.12	0.16 / 0.11	0.05 / 0.04
V[bvs]	0.11 / 0.11	0.10 / 0.11	0.03 / 0.04
V[col]	0.19 / 0.17	0.18 / 0.17	0.06 / 0.06
L[cmy]	0.14 / 0.11	0.13 / 0.11	0.04 / 0.04
L[bvs]	0.12 / 0.08	0.11 / 0.08	0.04 / 0.03
S[cmy]	0.16 / 0.07	0.15 / 0.07	0.05 / 0.02
S[bvs]	0.19 / 0.14	0.19 / 0.13	0.06 / 0.04
□[bvs]	0.16 / 0.16	0.15 / 0.16	0.05 / 0.05
ā[cmy]	0.05 / 0.05	0.05 / 0.04	0.02 / 0.01

*CV*tot, total coefficient of variation; *CV*biol, biological coefficient of variation; *CE*met, coefficient of error of the stereological procedure

Results

Biometrical Analysis

The initial (362.68 ± 31.19g; CV= 0.09) and final (503.83 ± 27.00g; CV= 0.05) body mass of the animals used in this study was similar in both groups, with no significant difference. There was also no significant difference between the RA volume in the CG (113.58 ± 7.01mm^3, CV= 0.06) and IG (117.31 ± 5.14mm^3, CV= 0.04) animals. The LV volume was significantly higher in IG animals (487.69 ± 34.89mm^3, CV= 0.07) compared with CG animals (456.47 ± 26.18mm^3, CV= 0.06).

Myocardial Histopathology and stereology

Myocardial pathological changes were evident in the RA and LV after nine weeks of *T. cruzi* infection. Infected animals showed intracellular *T. cruzi* amastigote nests and intense diffuse inflammatory infiltrates with a predominance of mononuclear cells (Fig. 1). The density of mononuclear cells and polymorphonuclear cells was significantly higher in the RA and LV myocardium of IG animals compared to the CG animals (Table 2). For the IG animals, cellular atrophy was identified with cardiomyocytes showing pyknotic nuclei, marked cytoplasmic fragmentation, intense and diffuse myocardial fibrosis and tissue necrosis. These characteristics were not observed in the CG animals (Fig. 1).

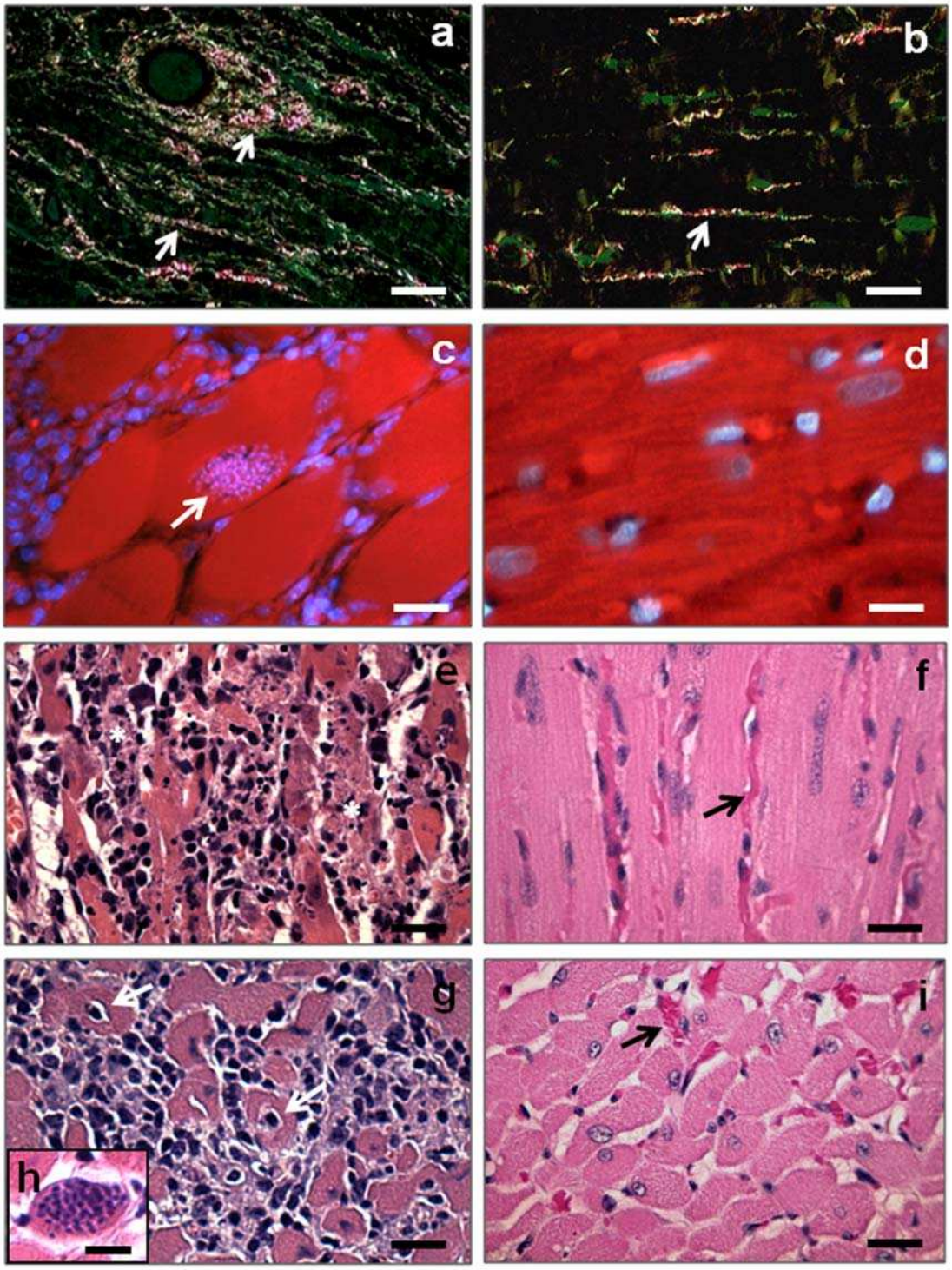

Fig. 1 Representative photomicrographs of the left ventricle from infected (a, c, e, g and h) and control (b, d, f and i) rats. (a) Intense deposition of collagen fibers (arrows) with pericellular and perivascular distribution in the myocardium of infected animals (Sirius red staining under polarized light microscopy, bar = 30µm). (b) A lower density of collagen fibers is observed in the control group (Sirius red staining under polarized light microscopy, bar = 30µm). (e) A large area of necrosis with cardiomyocytes fragmentation (asterisks) and intense leukocyte infiltration are observed in the myocardium of infected

animals. In these animals a myocardial cross-section shows cardiomyocytes with reduced diameters, pyknotic nuclei (arrow) and diffuse inflammatory infiltrates (g) (H&E staining, bar = 30μm). Detail of an intracellular nest of *T. cruzi* is observed in (c) (DAPI and Phaloidin staining under epifluorescence microscopy, bar = 20μm) and (h) (H&E staining, bar = 30μm). For the control animals (d, f and i) the myocardium showed a well-organized structure. Blood capillaries are indicated by the arrows (H&E staining, bar = 30μm)

Table 2 Stereological parameters and cellularity of the myocardium from control and infected rats

Parameter	Control	Infected
Right atrium		
V[col] (mm^3)	9.37 ± 2.13	15.62 ± 2.80*
V[bvs] / V[cmy]	0.14 ± 0.01	0.18 ± 0.02*
V[int] / V[cmy]	0.52 ± 0.11	0.82 ± 0.20*
ā[cmy] (μm^2)	52.20 ± 8.84	36.36 ± 5.12*
□[bvs] (μm^2)	5.45 ± 0.27	5.29 ± 0.31
MN cell (N/170×10^3 μm^2)	71.27 ± 17.65	279.12 ± 34.01*
PMN cell (N/170×10^3 μm^2)	29.86 ± 16.05	77.25 ± 18.85*
Left ventricle		
V[col] (mm^3)	29.56 ± 5.40	49.67 ± 8.16*
V[bvs] / V[cmy]	0.16 ± 0.03	0.24 ± 0.03*
V[int] / V[cmy]	0.43 ± 0.07	0.81 ± 0.19*
ā[cmy] (μm^2)	52.78 ± 8.83	36.65 ± 5.84*
□[bvs] (μm^2)	5.28 ± 0.25	4.89 ± 0.22*
MN cell (N/170×10^3 μm^2)	68.62 ± 19.49	302.70 ± 40.57*
PMN cell (N/170×10^3 μm^2)	25.47 ± 14.51	172.92 ± 17.36*

V[col], total volume of collagen fibers; ā[cmy], mean cross-sectional area of cardiomyocytes; □[bvs], mean diffusion distance; MN, mononuclear cells; PMN, Polimorphonuclear cells. The data are represented as mean ± S.D. *Denotes statistical difference from control for the same segment ($P < 0.001$), student t-test.

The IG animals presented a significant reduction of the total volume and the total length occupied by cardiomyocytes in the RA and LV compared to the CG animals (Fig. 2). Conversely, the total interstitial volume and the total collagen volume were significantly increased in the RA and LV of IG animals (Table 2 and Fig. 2). The total volume and total length of blood vessels was significantly increased only in the LV of IG animals (Fig. 2 and 3).

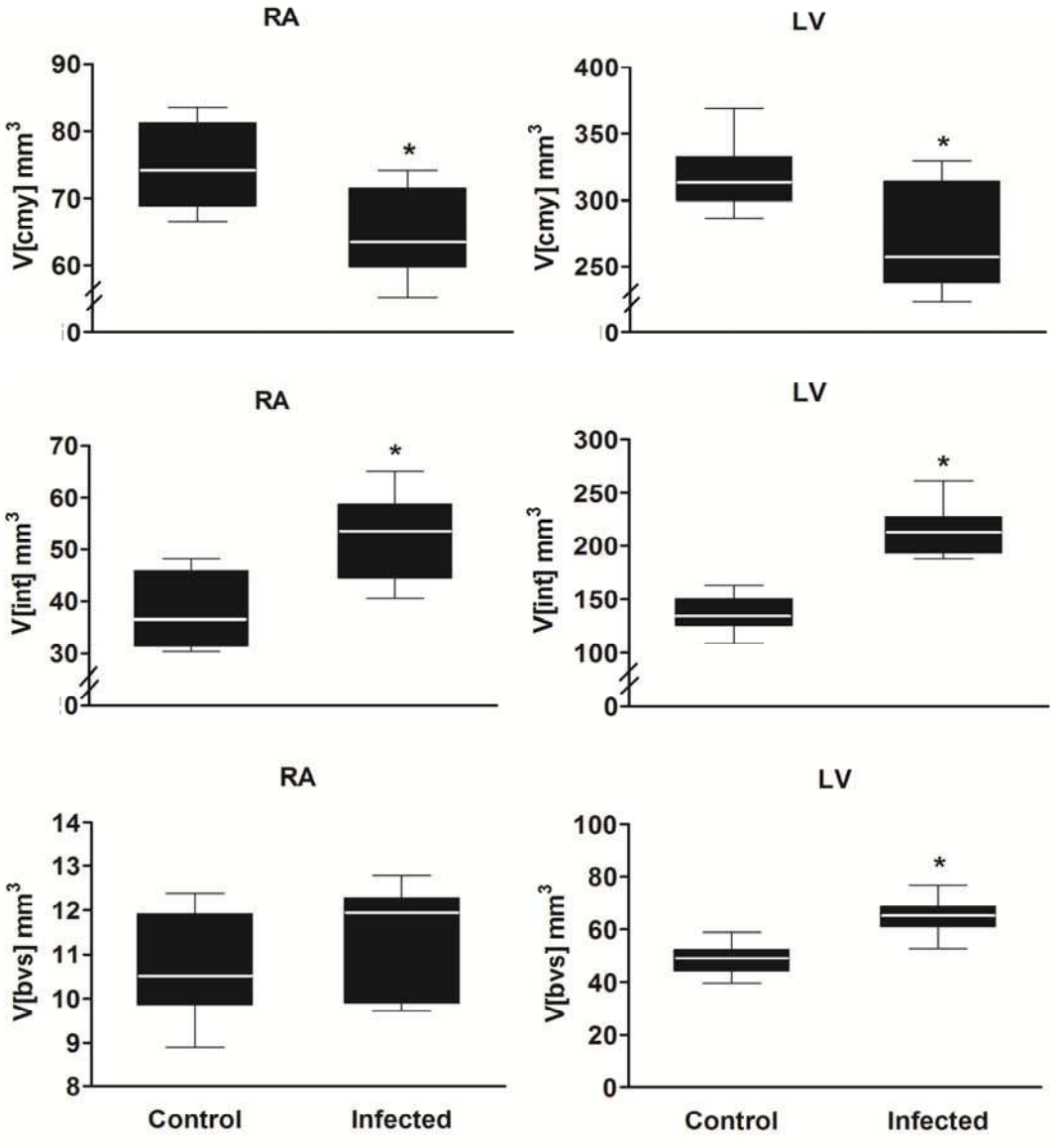

Fig. 2 Total volume occupied by cardiomyocytes (V[*cmy*]), interstitium (V[*int*]) and blood vessels (V[bvs]) in the right atrium (RA) and left ventricle (LV) from control and infected rats. The box represents the interquartile interval with the median indicated (horizontal line), and whiskers represent the superior and inferior quartiles. *Denotes statistical difference from control ($P < 0.001$) for the same segment, Mann-Whitney U test

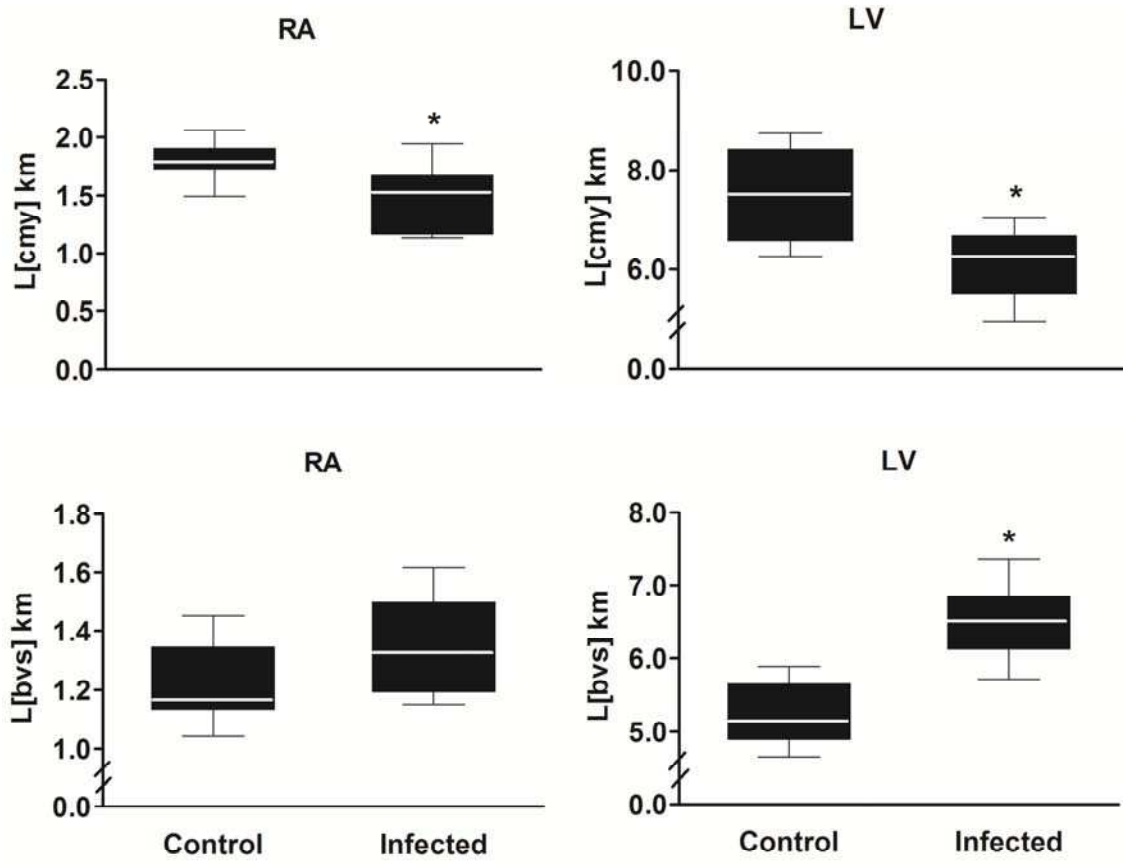

Fig. 3 Total length of cardiomyocytes (L[cmy]) and blood vessels (L[bvs]) in the right atrium (RA) and left ventricle (LV) from control and infected rats. The box represents the interquartile interval with the median indicated (horizontal line), and whiskers represent the superior and inferior quartiles. *Denotes statistical difference from control ($P < 0.001$) for the same segment, Mann-Whitney U test

Infected animals presented with a significant reduction of the total surface area and mean cross-sectional area of cardiomyocytes in the RA and LV and total blood vessel surface area in the RA compared to CG animals (Table 2 and Fig. 4). The total surface area of blood vessels was significantly higher in the LV of IG animals (Fig. 4). The mean diffusion distance from the capillary to tissue was similar for both groups (Table 2).

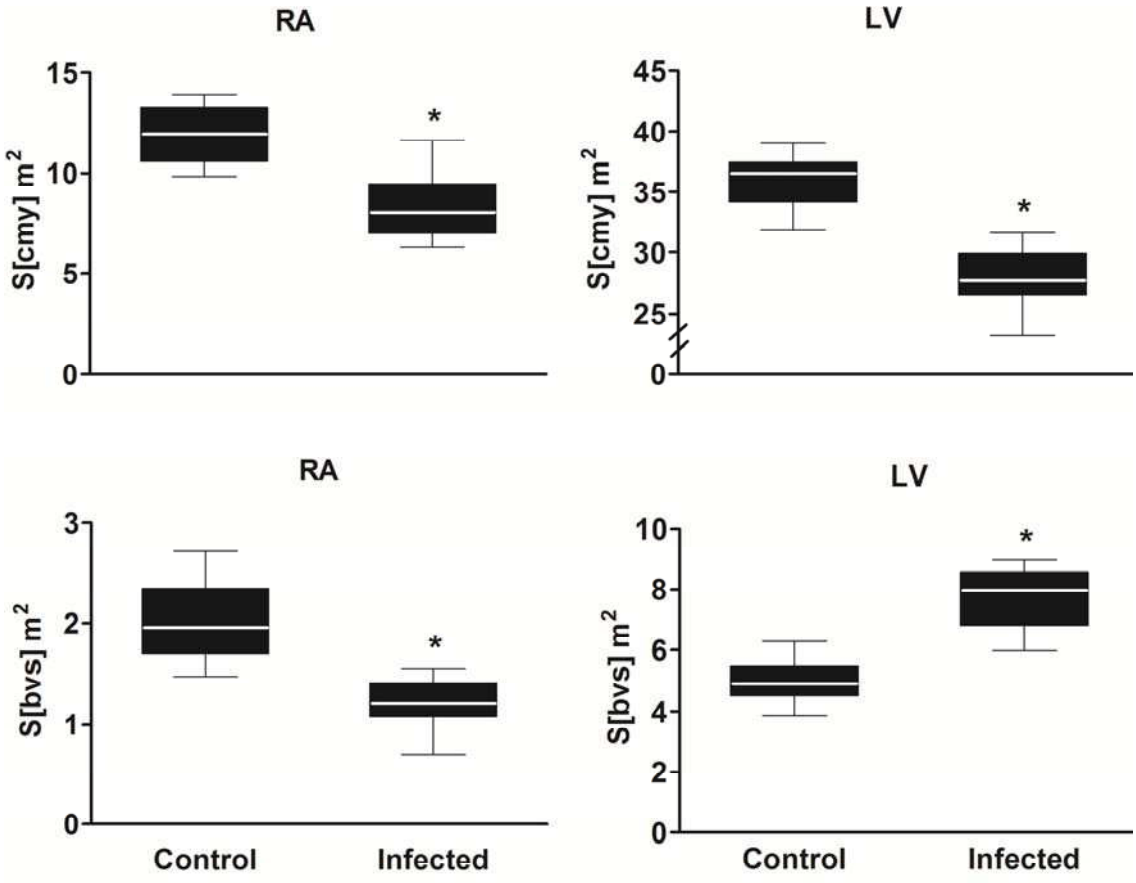

Fig. 4 Total surface area of cardiomyocytes (S[cmy]) and blood vessels (S[bvs]) in the right atrium (RA) and left ventricle (LV) from control and infected rats. The box represents the interquartile interval with the median indicated (horizontal line), and whiskers represent the superior and inferior quartiles. *Denotes statistical difference from control ($P < 0.001$) for the same segment, Mann-Whitney U test

Cardiomyocytes contractility

The analysis of cell contractility showed marked changes in the mechanical properties of isolated cardiomyocytes from IG animals (Fig. 5). In this group, RA and LV cardiomyocytes presented with a significant reduction in cell shortening (43.02% and 24.98%, respectively) compared to the CG animals. The curve of cell contractility as a function of time showed a lower amplitude of variation of cell length in IG animals (Fig. 5). In addition, RA and LV cardiomyocytes had a significant prolongation of the time to the peak of contraction (17.09%) and the time to half relaxation (23.68%) in relation to the CG animals. These results are also indicated by a marked prolongation of the relaxation

and contraction components in the curve of cell contractility relative to the RA and LV, respectively (Fig. 5).

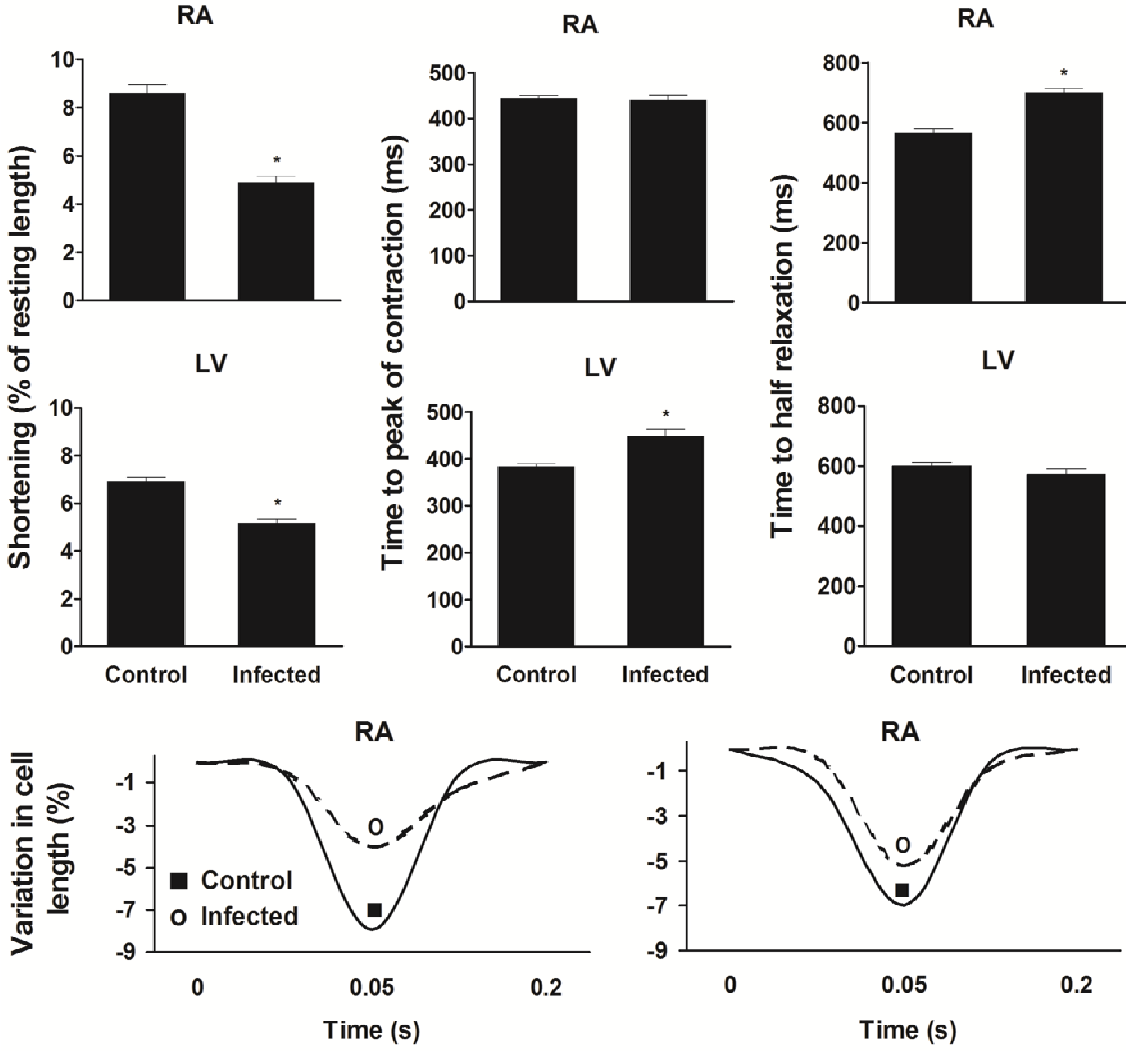

Fig. 5 Contractility parameters of cardiomyocytes of the right atrium (RA) and left ventricle (LV) from control and infected rats. The data are represented as mean ± S.D. *Denotes statistical difference from control ($P < 0.001$) for the same segment, student t-

Mineral microanalysis and lipid peroxidation

The mineral concentration in the RA and LV was similar in both groups investigated, with no statistical difference between them (Fig. 6). The biochemical analysis indicated a significant increase in lipid hydroperoxide (HPX) levels in the RA and LV from IG animals compared to the CG animals (Fig. 7a). The linear regression analysis showed a moderate and significant inverse correlation between the amplitude of cell shortening and

the lipid HPX levels in the RA and LV from IG animals (Fig 6c). The correlation was not significant for CG animals.

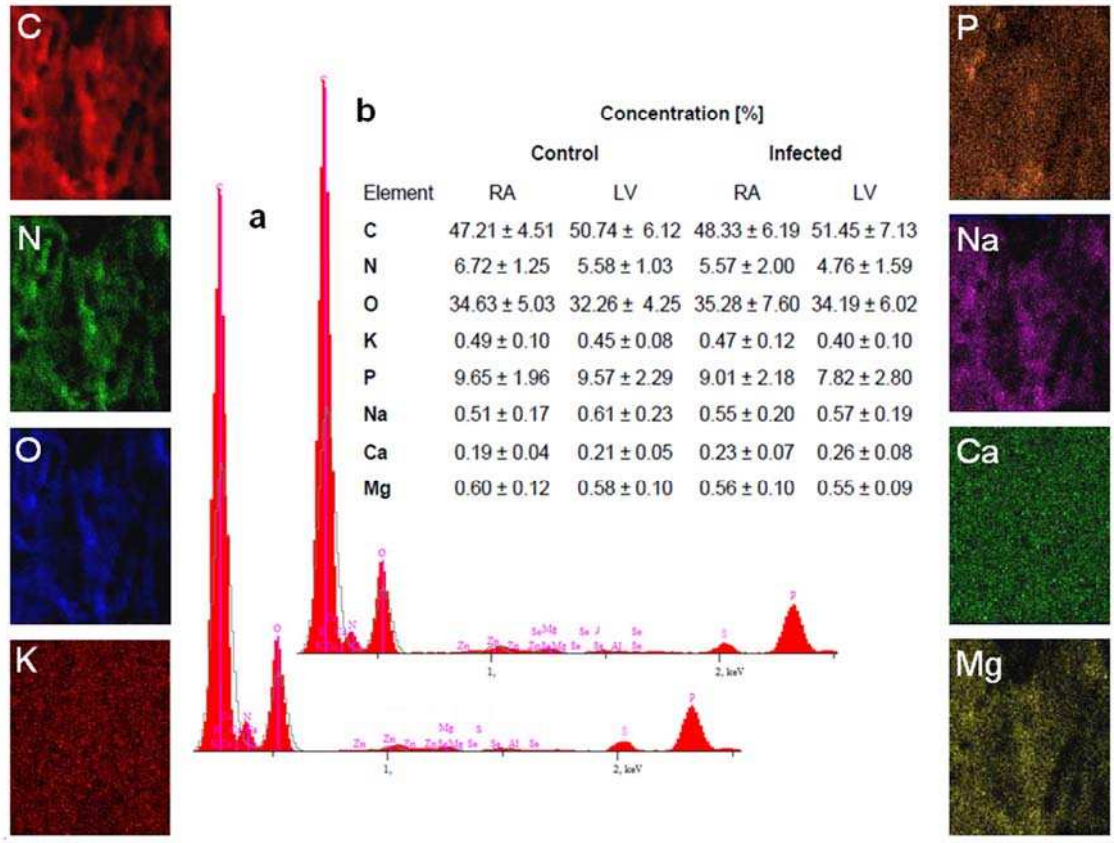

Fig. 6 Mineral content in the right atrium (RA) and left ventricle (LV) of control and infected rats. The images in the left and right columns represent the mineral distribution map in the LV from control animals. In some images can be seen a cardiomyocyte profile. A representative spectrum of Energy Dispersive X-ray Spectroscopy is shown for each mineral in the LV from control (a) and infected (b) animals. The numbers (mean ± S.D) represent the proportion of minerals in the RA and LV for both groups. *There was no significant difference in the mineral proportion for each cardiac segment between the groups ($P > 0.05$), student t-test

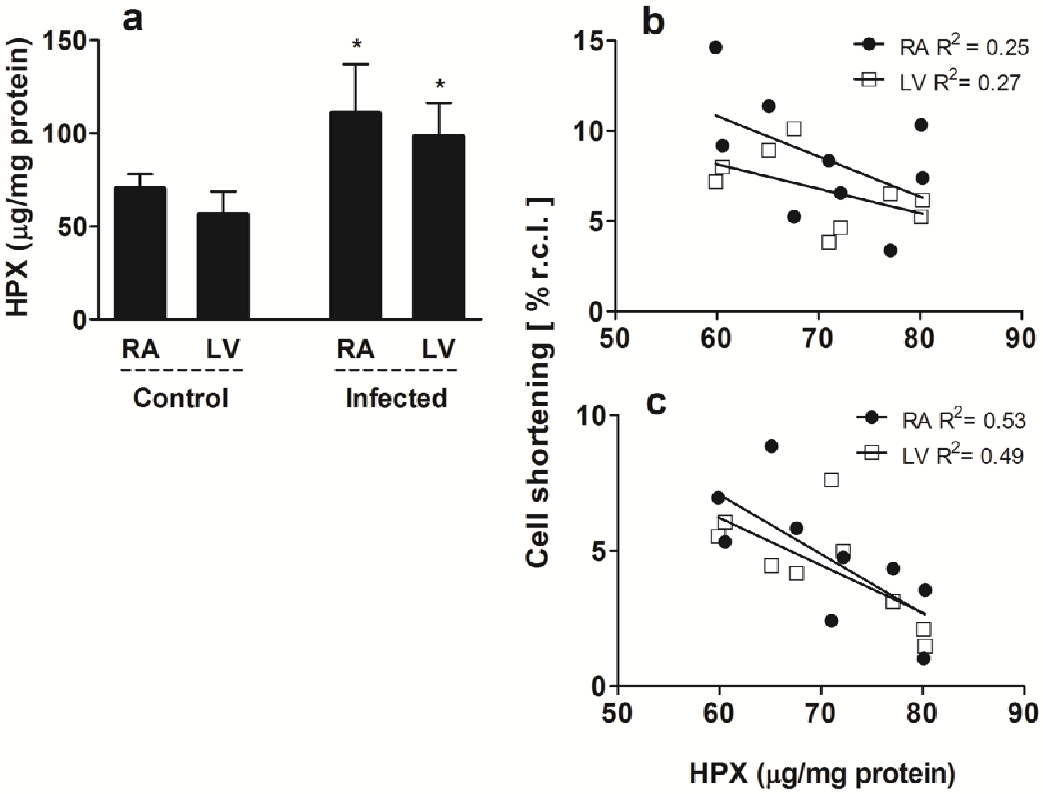

Fig. 7 Tissue levels of lipid hydroperoxides (HPX) and correlations between HPX and cell shortening in the right atrium (RA) and left ventricle (LV) from control (b) and infected (c) rats. In (a), the data are represented as mean ± S.D. In (b) and (c), the mean of cell shortening per animal was plotted against the HPX levels in each cardiac segment for both groups. Shortening is expressed as % of resting cell length (% r.c.l.). *Denotes statistical difference from the control ($P < 0.001$) for the same segment, student t-test

Discussion

In the present study, infection was induced using a *T. cruzi* Y strain due to its high virulence and tropism by cardiac tissue (Novaes et al. 2011; 2012). The results showed that the standardized inoculum and the consequential *T. cruzi* infection were sufficient to stimulate lipid peroxidation, induce marked myocardial morphological reorganization and cardiomyocyte contractile dysfunction.

The present study showed that *T. cruzi* infection induced marked RA and LV structural remodeling. Using design-based stereology methods it was possible to identify for the first time that this remodeling extends beyond the focal or relative features considered pathognomonic of ChC, such as cell parasitism, mononuclear inflammatory infiltrate,

microvascular constriction, fibrosis, cardiomyocitolysis and necrosis (Higuchi et al. 1993; Rossi, 1998; Rossi et al. 2010). Taken together, the stereological data indicated that the pathological reorganization of the myocardial stroma and parenchyma changes the global histoarchitecture of the RA and LV. Interestingly, although an evident reduction in total cardiomyocyte volume has been observed, the RA and LV volume were not reduced in IG animals. This finding clearly demonstrates the adaptability of the myocardial stroma in response to the parenchymal damage. Thus, the reactive expansion of the extracellular matrix components, especially through collagenogenesis and neoangiogenesis, represents important processes related to the cardiac remodeling in ChC, which is evident in the replacement of functional components by structural myocardial components (Rossi et al. 1998; Higuchi et al. 1993, 1999; Marin-Neto et al. 2007).

Recently, studies conducted in our laboratory have clarified new aspects of the ChC pathogenesis (Roman-Campos et al. 2009; Novaes et al. 2011; Novaes et al. 2012). These studies indicate for the first time that the deterioration of cardiac function observed in the acute and chronic phases of ChC represents a cellular basis related to cardiomyocyte mechanical insufficiency. In the present study, temporal and spatial evidence of contractile incompetence were observed in the cardiomyocytes that resisted infection. Interestingly, dysfunctional cardiomyocytes were isolated from infected RA and LV myocardium presenting a completely altered structural microenvironment. In fact, the myocardial volume occupied by cardiomyocytes was decreased and the ECM volume (V[int]) was markedly increased in the RA and LV. However, the volume occupied by blood vessels was only increased in the LV. Moreover, interestingly, LV cardiomyocytes from IG animals had higher contractile amplitudes compared to the RA cardiomyocytes, suggesting a possible relationship between tissue vascularization and cardiomyocyte mechanical function. The presence of microvascular damage, such as thrombosis, vascular constriction and collapse, necrosis and derangement of the myocardial vascular network, is not unusual in ChC (Higuchi et al. 1999; Biolo et al. 2010; Rossi et al. 2010; Novaes et al. 2011). There is evidence that the reduction in myocardial vascularization constitutes an important component involved in the deterioration of cardiac function in ChC (Higuchi et al. 1999; Marin-Neto et al. 2007). Thus, the occurrence of an abnormal heart rhythm with the onset of electrical abnormalities such as complex arrhythmias and cardiac pump dysfunction are serious consequences of the myocardial hypoperfusion that decreases the mechanical efficiency of the heart (Verani et al. 1981; Meiler et al. 1987). These findings point to the close association between the cell and the extracellular matrix (ECM), in which complex

and synergic relationships are indispensable to the maintenance of cardiac homeostasis (Ingber, 2002; Brutsaert, 2003; Kresh and, Chopra, 2011). There is sufficient evidence that different components of the ECM modulate several signaling pathways to control and maintain cardiac metabolism, growth, cellular and muscular contractile performance, and rhythmicity (Brutsaert, 2003; Parker and Ingber, 2007; Kresh and Chopra, 2011). Thus, the ECM creates a complex and finely tuned balance of cell interactions with the immediate environment. However, differences in the set point of this balance induced by regional or global pathological changes of the ECM result in substantial adaptations to the functional phenotype of cardiomyocytes, resulting in different spectra of cardiac dysfunction (Ingber, 2002; Brutsaert, 2003; Kresh and Chopra, 2011).

Considering the integration of cardiomyocytes with the ECM, it is not unrealistic to assume that the structural pathological remodeling of the myocardium induced by *T. cruzi* infection could potentially modify the molecular characteristics and physical properties of the ECM and subsequently impair the mechanisms that regulate the cellular contractile behavior, including mechanotransduction (Ingber, 2002; Parker and Ingber, 2007). However, several aspects of the cellular and molecular basis of these changes remain to be clarified and require further investigation. On the other hand, the relationship between cardiac structure, cellular function and heart function, indicates that the pathological RA and LV myocardial remodeling observed in ChC may have several negative consequences, such as hypertrophy, and hemodynamic, electrical and mechanical cardiac dysfunction (Mady et al. 1999; Marin-Neto et al. 2007; Lima et al. 2010a,b; Rassi-Jr et al. 2010; Santos et al. 2012). Thus, cardiomyocitolysis and tissue necrosis with progressive destruction and subsequent reconfiguration of the heart parenchyma and stroma can be associated with a reduction in the contractile force and cardiac stroke volume (Morris, 1990; Rossi, 1998; Mady et al. 1999; Rossi et al. 2010). The myocardial mechanical insufficiency is exacerbated by the extensive fibrosis that decreases the cardiac compliance and consequently decreases the efficiency of the frank-starling mechanism. This mechanism is essential for the modulation of cellular and muscular contraction forces (Kitzman et al. 1991; Higuchi et al. 1999), especially in conditions of autonomic denervation that are frequently seen in ChC (Morris et al. 1990; Biolo et al. 2010; Rossi et al. 2010). Moreover, the abnormal organization pattern of collagen fibers may decrease the contractile efficiency of the heart since part of the force used for pumping blood is diverted to correct the geometric distortion determined by the structural disorganization of collagen and possibly cardiomyocytes (Mady et al. 1999).

Previous studies have identified an important regulatory role of the ECM in the distribution of water and electrolytes in cardiac tissue, which can be markedly impaired in cardiomyopathies, especially when associated with tissue necrosis (Lehr, 1969; Toda, 1969). Moreover, it is widely recognized that tissue electrolyte concentrations, especially of calcium, sodium and potassium, modulate the cell membrane excitability and are critical for proper cardiomyocyte and whole heart contractile performance (Toda, 1969; Bers, 2001). Despite the intense pathological remodeling of the ECM, the minerals investigated in the RA and LV were distributed in similar proportions in both groups, a finding that reduced the influence of a possible tissue electrolytic imbalance on the results of cell contractility.

It has been systematically shown that reactive oxygen species (ROS) have potent effects on cardiomyocytes and the ECM. ROS can lead to irreversible cell damage or death, and can stimulate cardiac fibroblast proliferation, matrix metalloproteinase synthesis, ECM remodeling and fibrosis (Dhalla et al. 2000; Wen et al. 2008). Increased ROS production, including that by lipid hydroperoxides, has been involved in the progression of cardiac dysfunction observed in heart diseases with different etiologies, such as diabetes mellitus, hypertension (Dhalla et al. 2000), and *T. cruzi* infection (Wen and Garg, 2004; Wen et al. 2004, 2008; Gupta et al. 2009). Growing evidence highlights ROS as important inducers of cardiomyocyte contractile dysfunction (Xu et al. 1997; Kaplan et al. 2003; Gupta et al. 2009). The increased HPX levels in the RA and LV of IG animals and the inverse and moderate correlation between cell shortening and HPX levels corroborate these findings, suggesting a possible participation of lipid peroxidation in the pathogenesis of the myocardial structural remodeling and the mechanical dysfunction of cardiomyocyte in ChC. The relationship between oxidative stress and cardiomyocyte mechanical insufficiency has been suggested since ROS directly influence contractile function by modifying proteins that modulate the excitation-contraction coupling. This includes the modification of thiol radicals on the ryanodine receptor, the suppression of L-type calcium channel currents and the oxidative inhibition of sarcoplasmic reticular Ca2+ ATPase and Ca2+ uptake (Xu et al. 1997; Kaplan et al. 2003). Moreover, previous studies showed that *T. cruzi* infection stimulates the production of free radicals and causes a dysfunction in the cellular metabolism of energy via the uncoupling of several enzymatic complexes that are integrated with the electron transport chain (Wen and Garg, 2004; Wen et al. 2008; Gupta et al. 2009). However, the relationship of these molecular changes with myocardial

structural remodeling and the cellular mechanics of *T. cruzi* infection are poorly understood and require further investigation.

In summary, the results indicate that *T. cruzi* infection induces global and pathological structural remodeling of the RA and LV myocardium. This remodeling does not influence the myocardial mineral concentration but coexists with cardiomyocyte contractility dysfunction, which was possibly related to a new and abnormal organization pattern of the myocardial stroma and the increased cellular lipid peroxidation.

Acknowledgements

The authors would like to acknowledge the "*Núcleo de Microscopia e Microanálise*" of the Federal University of Viçosa (UFV). Rômulo D. Novaes was a recipient of the PhD scholarship from CAPES. Antônio J. Natali and André Talvani are CNPq fellows.

References

Aherne WA (1967) Methods of counting discrete tissue components in microscopical sections. J R Micr Soc 87:493-501.

Bers DM (2001) Cardiac excitation–contraction coupling. Nature 415:198-205.

Biolo A, Ribeiro AL, Clausell N (2010) Chagas cardiomyopathy-where do we stand after a hundred years? Prog Cardiovasc Dis 52:300-316.

Bradford M (1976) A rapid and sensitive method for quantitation of microgram quantities of protein utilizing the principle of protein-dye-binding. Anal Biochem 72:248-254.

Brener Z (1962) Therapeutic activity and criterion of cure on mice experimentally infected with *Trypanosoma cruzi*. Rev Inst Med Trop São Paulo 4:389-396.

Brüel A, Oxlund H, Nyengaard JR (2005) The total length of myocytes and capillaries, and total number of myocyte nuclei in the rat heart are time dependently increased by growth hormone. Growth Horm IGF Res 15:256-264.

Brutsaert DL (2003) Cardiac endothelial-myocardial signaling: its role in cardiac growth, contractile performance, and rhythmicity. Physiol Rev 83:59-115.

Cruz-Orive LM, Weibel ER (1990) Recent stereological methods for cell biology: a brief survey. Am J Physiol 25:8148-8156.

Dhalla NS, Temsah R, Netticadan T (2000) Role of oxidative stress in cardiovascular diseases. J Hypertens 18:655–673.

Dorph-Petersen KA, Nyengaard JR, Gundersen HJ (2001) Tissue shrinkage and unbiased stereological estimation of particle number and size. J Microsc 204:232-246.

Guerri-Guttemberg RA, Grana DR, Ambrosio G, Milei J (2008) Chagas cardiomyopathy: Europe is not spared!. Eur Heart J 29:2587-2591.

Gupta S, Bhatia V, Wen JJ, Wu Y, Huang MH, Garg NJ (2009) *Trypanosoma cruzi* infection disturbs mitochondrial membrane potential and ROS production rate in cardiomyocytes. Free Radic Biol Med 47:1414-1421.

Gupta S, Wen J, Garg NJ (2009) Oxidative stress in Chagas disease. Interdiscip Perspect Infect Dis 1-8; ID190354.

Higuchi ML, Brito T, Reis MM, Barbosa A, Bellotti G, Pereira-Barreto AC, Pileggi F (1993) Correlation between *Trypanosoma cruzi* parasitism and myocardial inflammatory infiltrate in human chronic chagasic myocarditis: light microscopy and immunohistochemical findings. Cardiovasc Path 2:101-106.

Higuchi ML, Fukasawa S, Brito T, Parzianello LC, Bellotti G, Ramires JAF (1999) Different microcirculatory and interstitial matrix patterns in idiopathic dilated cardiomyopathy and Chagas' disease: a three dimensional confocal microscopy study. Heart 82:279-285.

Ingber DE (2002) Mechanical signaling and the cellular response to extracellular matrix in angiogenesis and cardiovascular physiology. Circ Res 91:877-887.

Kaplan P, Babusikova E, Lehotsky J, Dobrota D (2003) Free radical-induced protein modification and inhibition of Ca2+-ATPase of cardiac sarcoplasmic reticulum. Mol Cell Biochem. 248:41-47.

Kitzman DW, Higginbotham MB, Cobb FR, Sheikh KH, Sullivan MJ (1991) Exercise intolerance in patients with heart failure and preserved left ventricular systolic function: failure of the Frank-Starling mechanism. J Am Coll Cardiol 17:1065-1072.

Kresh JY, Chopra A (2011) Intercellular and extracellular mechanotransduction in cardiac myocytes. Pflugers Arch 462:75-87.

Lehr D (1969) Tissue electrolyte alteration in disseminated myocardial necrosis. Ann N Y Acad Sci 156:344-78.

Lima MM, Rocha MO, Nunes MC, Sousa L, Costa HS, Alencar MC, Britto RR, Ribeiro AL (2010a) A randomized trial of the effects of exercise training in Chagas cardiomyopathy. Eur J Heart Fail 12:866-873.

Lima MM, Nunes MC, Rocha MO, Beloti FR, Alencar MC, Ribeiro AL (2010b) Left ventricular diastolic function and exercise capacity in patients with Chagas cardiomyopathy. Echocardiography 27:519-24.

Mady C, Ianni BM, Arteaga E, Montes GS, Caldini EG, Andrade G, Giorgi MC, Saldiva PH (1999) Relation between interstitial myocardial collagen and the degree of clinical impairment in Chagas' disease. Am J Cardiol 84:354-356.

Mandarim-de-Lacerda CA (2003) Stereological tools in biomedical research. An Acad Braz Sci 75:469-486.

Marin-Neto JA, Cunha-Neto E, Maciel BC, Simões MV (2007) Pathogenesis of chronic Chagas' heart disease. Circulation 115:1109-1123.

Morris SA, Tanowitz HB, Wittner M, Bilezikian JP (1990) Pathophysiological insights into the cardiomyopathy of Chagas' disease. Circulation 82:1900-1909.

Natali AJ, Wilson LA, Peckham M, Turner DL, Harrison SM, White E (2002) Different regional effects of voluntary exercise on the mechanical and electrical properties of rat ventricular myocytes. J Physiol 541:863-875.

Nourooz-Zadeh J, Tajaddini-Sarmadi J, Wolf SP (1994) Measurement of plasma hydroperoxide concentrations by the ferrous oxidation-xilenol orange assay in conjunction with thiphenylphosphine. Anal Biochem 220:403-409.

Novaes RD, Penitente AR, Gonçalves RV, Talvani A, Neves CA, Maldonado IR, Natali AJ (2011) Effects of *Trypanosoma cruzi* infection on myocardial morphology, single cardiomyocyte contractile function and exercise tolerance in rats. Int J Exp Pathol 92:299-307.

Novaes RD, Penitente AR, Talvani A, Natali AJ, Neves CA, Maldonado IRSC (2012) Use of fluorescence in a modified disector method to estimate the number of myocytes in cardiac tissue. Arq Bras Cardiol 98:252-258.

Parker KK, Ingber DE (2007) Extracellular matrix, mechanotransduction and structural hierarchies in heart tissue engineering. Phil Trans R Soc B 362:1267-1279.

Rassi-Jr A, Rassi A, Marin-Neto JA (2010) Chagas disease. Lancet 375:1388-1402.

Roman-Campos D, Duarte HLL, Sales-Jr PA, Natali AJ, Ropert C, Gazzinelli RT, Cruz, JS (2009) Changes in cellular contractility and cytokines profile during *Trypanosoma cruzi* infection in mice. Basic Res Cardiol 104:238-246.

Rossi MA, Tanowitz HB, Malvestio LM, Celes MR, Campos EC, Blefari V, Prado CM (2010) Coronary microvascular disease in chronic chagas cardiomyopathy including an overview on history, pathology, and other proposed pathogenic mechanisms. Plos Negl Trop Dis 4:1-12.

Rossi MA (1998) Fibrosis and inflammatory cells in human chronic chagasic myocarditis: scanning electron microscopy and immunohistochemical observations. Int J Cardiol 66:183-194.

Santos FM, Lima WG, Gravel AS, Martins TA, Talvani A, Torres RM, Bahia MT (2012) Cardiomyopathy prognosis after benznidazole treatment in chronic canine Chagas' disease. J Antimicrob Chemother [Epub ahead of print]

Scherle W (1970) A simple method for volumetry of organs in quantitative stereology. Mikroskopie 26:57-63.

Toda N (1969) Effects of calcium, sodium and potassium ions on contractility of isolated atria and their responses to noradrenaline. Br J Pharmacol 36:350-367.

Xu KY, Zweier JL, Becker LC (1997) Hydroxyl radical inhibits sarcoplasmic reticulum Ca2+-ATPase function by direct attack on the ATP binding site. Circulation Res 80:76-81.

Wen J, Dhiman M, Whorton EB, Garg NJ (2008) Tissue-specific oxidative imbalance and mitochondrial dysfunction during *Trypanosoma cruzi* infection in mice. Microbes Infect 10:1201-1209.

Wen J, Garg N (2004) Oxidative modification of mitochondrial respiratory complexes in response to the stress of *Trypanosoma cruzi* infection. Free Radic Biol Med 37:2072-2081.

PERSPECTIVAS

Alterações patológicas do miocárdio e deterioração das propriedades contráteis de cardiomiócitos foram encontradas no presente estudo. Até o momento, pouco se sabe a respeito dos mecanismos por meio dos quais o *T. cruzi* atua para alterar a contratilidade. Existem dados na literatura que indicam influência do sistema imunológico na modulação da contratilidade celular em cardiopatias de origem não chagásica. Entretanto, a contribuição do sistema imunológico na disfunção mecânica celular evidenciada na doença de Chagas permanece pouco conhecida e requer novos estudos, principalmente em relação ao papel das citocinas e quimiocinas na modulação da contratilidade celular.

Embora a investigação das alterações da morfologia cardíaca e mecânica celular possam contribuir para o conhecimento atual da cardiopatia chagásica e explicar parcialmente a redução da tolerância ao exercício físico, ainda existem questionamentos a respeito dos fatores que limitam a capacidade de realizar exercícios físicos na doença de Chagas, visto que trata-se de uma doença sistêmica. Nesse contexto, elementos morfo-funcionais de outros sistemas que são comprometidos na infecção com *T. cruzi* e que estão direta ou indiretamente envolvidos nos ajustes requeridos à prática de exercícios físicos devem ser adicionalmente investigados. Abordagem especial deve ser direcionada aos músculos esqueléticos e pâncreas uma vez que apresentam relação direta com o metabolismo energético e a conversão de energia em trabalho físico. Nesse contexto, a análise da função pancreática, metabolismo de glicose e suas vias de utilização pelos músculos exercitados podem fornecer novas informações sobre os mecanismos por meio dos quais a infecção com *T. cruzi* modifica a tolerância ao exercício físico.